

Active reduction of noise transmitted into and from enclosures through encapsulated structures.

Marie Skłodowska-Curie Actions

project no. 101073037

D1.2 / D2

Review and results validation on integration on active casings based on distributed architecture with remote sensing WP1 – Device noise reduction (in-out problem)

Lead beneficiary: UOS

Date and version: 31/01/2025 v1.1

Type: Report

Dissemination level: Public







Abstract

The report related to milestone no. 8: Review and results validation on integration on active casings based on distributed architecture with remote sensing.

Although noise reduction in casings through active control methods appears plausible and promising, the benefits of these methods may still be constrained by computational complexity and physical design limitations. This report highlights recent advancements addressing these challenges and discusses specific developments, such as the use of distributed architectures and remote sensing techniques, to enable the practical implementation of active control methods.

Table of Contents

1	Intr	oduction	4								
2	Acti	Active control of casings									
	2.1 Casing used for active control										
	2.2 Non-distributive adaptive control algorithms										
		2.2.1 Multiple-Error FxLMS (MEFxLMS) algorithm	8								
		2.2.2 Other non-distributive control algorithms used in active casings	ç								
3	A re	eview of distributed algorithms for active control system	12								
	3.1	Introduction of distributed networks	12								
	3.2	Distributed MEFxLMS (DMEFxLMS) algorithm for ANC	13								
	3.3	Other distributed algorithms used in ANC	15								
4	Virt	ual sensing techniques	18								
	4.1	Virtual Microphone Arrangement	19								
	4.2	Remote Microphone Technique	20								
	4.3	Virtual Microphone Control - Additional Filter	22								
	4.4	Kalman filtering	24								
5	Inte	gration of virtual sensings and its distributed control algorithms in active casings	28								
	5.1	Distributed control system implemented in active casings	28								
	5.2	Virtual Sensing Method for Active casing	31								
6	Con	clusion	41								
Ri	hlino	rranhv	41								

Chapter 1

Introduction

Prolonged exposure to environmental noise has become a growing concern due to its detrimental effects on human health that encompass both auditory and non-auditory impacts [1]. Significant research would be required to reduce these noise levels. In general, mitigation measures for noise pollution can be implemented at the noise source, along the propagation paths, or at the receiver's end. Although there are various strategies available, each approach comes with its own set of challenges and limitations. Source-based measures, such as quieter machinery or operational changes, are often the most effective but can be difficult to implement, as they typically involve multiple stakeholders. Measures along the propagation paths, such as noise barriers or sound-proof windows, can reduce noise levels but may require significant investment and space. Finally, noise can be mitigated at the receiver's end, such as personal protective equipment. While this method may be the easiest to implement and therefore the most practical, it does not address the root cause of the problem. This report primarily focuses on noise mitigation methods applied at the source, in particular to noise-controlling casings that enclose the source in a sound-absorbing casing, thereby isolating it from its surroundings [2].

The noise reduction techniques typically utilised in a noise-controlling casing are classified to passive and active methods. Passive noise control (PNC) methods, which rely on sound insulation and absorption [3], typically require the material thickness to be of a similar order of magnitude as the acoustic wavelength. Consequently, PNC methods are generally more effective at high frequencies – although numerous prior studies have addressed this limitation by designing solutions specifically for lower frequencies, often making use of metamaterials [4]. In contrary, active noise control (ANC) methods use secondary loudspeakers that generate a counteracting signal, which is designed to create destructive interference with the unwanted sound within the targeted area [5]. This technique, on the other hand, will be more suited for lower frequency regions, since the global noise reduction performance will lose its effectiveness with an increasing frequency [6, 7]. Generally, these two methods are often combined together to give the best overall noise reduction across the frequency spectrum.

Although the concept of ANC systems was proposed as early as 1934 [8], with notable achievements in the 1950s [9, 10], significant challenges persisted during implementation. These challenges stemmed from the complexity and inflexibility of analogue circuits, as well as the complexity of debugging procedures with the electronics available at the time, making precise filter design exceedingly difficult. Even minor errors in phase or amplitude could lead to an unintended increase in





noise power rather than effective cancellation. This situation changed with the introduction of digital signal processors (DSP), driven by the rapid advancements in microelectronics and landmark algorithmic developments during the late 1970s and 1980s. Digital systems addressed the limitations of analogue circuitry by enabling adaptive filtering [11], which provided not only precise and stable performance but also the flexibility to dynamically adjust system parameters in a changing noise environment. The introduction of the filtered-x least mean squares (FxLMS) algorithm [12] enables effective adaptation of the control filter to minimise unwanted noise by accounting for secondary path dynamics, which helps avoid the potential instability that can arise when using conventional least mean square (LMS) algorithms in active noise control applications. These innovations marked a turning point in the evolution of ANC systems, making them practical for a wide range of applications, including noise-controlling casing. A more detailed review in the history and development of ANC systems can be found in the following papers [13, 14].

In the context of active noise-controlling casings, increasing the number of secondary sources and error sensors is often desirable for achieving better global noise reduction. However, implementing the FxLMS algorithm in a fully centralised multichannel system (also known as the Multiple Error FxLMS algorithm, MEFxLMS) can present practical challenges. Specifically, the computational and memory requirements of the multichannel FxLMS algorithm increase with the number of secondary sources and error sensors [5], potentially exceeding the computational capacity of current DSP units. When DSP hardware capabilities are limited, a more efficient algorithm becomes necessary. Although various algorithms, such as sparse adaptive filtering, can be used to reduce computational complexity [5], these approaches often involve trade-offs, such as a reduced convergence speed, which would be suboptimal in certain scenarios. One potential solution is to decentralise the controller, as originally proposed in [15], by distributing the computational load across multiple DSP units. However, purely decentralised architectures that lack collaboration or the exchange of local information across multiple processors may underperform compared to centralised systems, especially in scenarios where strong coupling exists between secondary sources and error sensors. In such cases, the absence of coordination can lead to suboptimal control performance. Distributed architectures [16] can mitigate this limitation by enabling network communication between multiple processors, as will be further explored in Chapter 3.

The second challenge in active casing applications lies in the placement of error sensors. To effectively suppress sound radiation, error sensors are typically required to be positioned away from the casing to monitor and control the acoustic noise. However, in some specific active casings, the placement of physical sensors is constrained to the surface of the casing, thereby limiting their effectiveness. In such scenarios, virtual sensing (VS) techniques [17] provide a practical solution by using signals from physical monitoring sensors to estimate error signals at remote locations. These techniques, which enable effective control despite physical limitations, will be explored in greater details in Chapter 4.

This report shall provide a review on the integration on active casing based on distributed architecture equipped with remote sensing. The report is structured as follows: Chapter 2 formally introduce the concept of active casings and some of the proposed non-distributive ANC algorithms used to reduce the computation complexity in the multichannel system; Chapter 3 and 4 shall discuss the distributed algorithm and virtual sensing techniques typically used in an active control system, respectively; Chapter 5 shall then discuss the integration of these techniques in an active casing; and Chapter 6 draws conclusion.

Chapter 2

Active control of casings

This chapter shall formally introduce the non-distributive active control methods used to reduce noise radiation coming out from an enclosed casing. Section 2.1 shall first describe the different types of casing used in control, as each of their characteristics will introduce different modeling complexities to the active control problem [2]. Section 2.2 shall then present the various non-distributive control algorithm commonly used in active casings.

2.1 Casing used for active control

The casings types can be characterized into rigid casing [2, 18] and light-weight casing [19, 20]. Finally, it can be applied to off-the-shelf devices as long as their casings' walls can be subjected to vibration forces (real casing) [21].

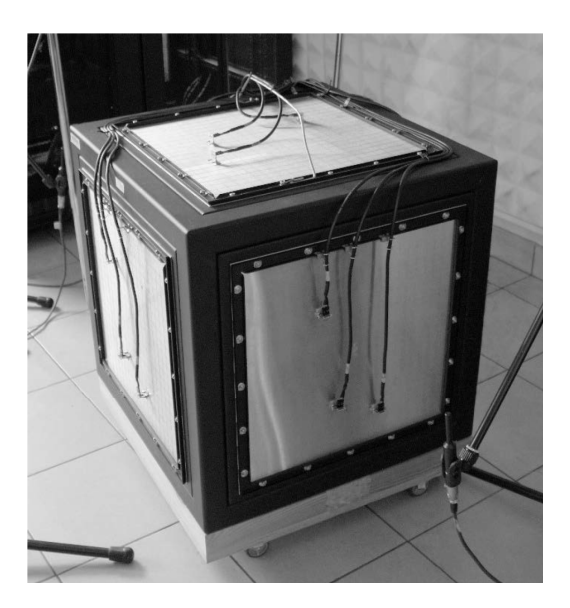


Figure 2.1: Photographs of the rigid active casing [22].





Rigid casings

In rigid casings, all walls are constructed using either single or double panels. Each panel is secured to the structure with screws embedded in the frame and clamped using an additional steel square frame (Figure 2.1).

Lightweight casings

The lightweight casing was constructed without a dedicated frame (Figure 2.2). This design led to increased vibrational coupling between the individual walls, as well as coupling through the acoustic field inside the casing and, to a lesser extent, the external field. Additionally, the absence of a rigid frame meant the walls were directly connected to each other, resulting in boundary conditions that no longer behaved as fully clamped. Instead, the boundary conditions were more accurately characterized as being elastically restrained against both rotation and translation.

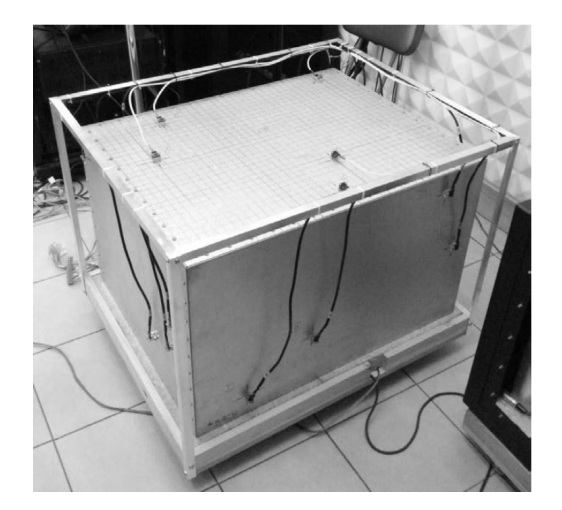




Figure 2.2: Photographs of the light-weight active casing [23].

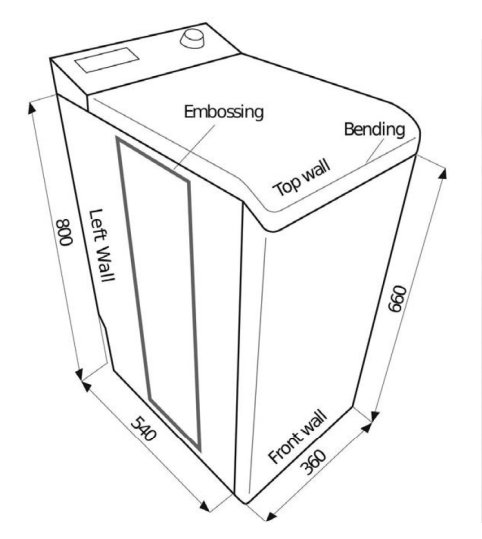




Figure 2.3: A Photograph and schematic of a real casing of a washing machine [24].





Real casings

Real casings refer to a real, mass-produced device casing. One of the most common examples is the washing machines (Figure 2.3). The real device casings are often highly irregular and inhomogeneous. Each wall exhibits distinct characteristics, such as bends, embossments, and other features, making it significantly more challenging to fit a mathematical model to each wall.

The casing forms a three-dimensional structure with strong couplings between the walls, similar to the lightweight casing. However, the unique nature of each wall and the structural separations are more apparent. To simplify the analysis, each wall is considered individually for determining actuator placement.

2.2 Non-distributive adaptive control algorithms

Noise-Controlling casings has been extensively enhanced and equipped with a variety of advanced control algorithms. The active control strategy used in the Noise-Controlling Casings primarily falls under the Active Structural Acoustic Control (ASAC), which primarily relies on a combination of passive noise barriers and vibration actuators [25, 26, 27]. By controlling structural vibrations, ASAC effectively reduces noise transmission. When carefully implemented, it not only minimizes noise in specific local areas but can also achieve global noise reduction [28].

The algorithms used to realize ASAC are similar to those in ANC systems. Section 2.2.1 provides an overview of the MEFxLMS algorithm commonly employed in ANC systems, followed by a discussion of non-distributive algorithms typically used to address computational complexity challenges in Section 2.2.2.

2.2.1 Multiple-Error FxLMS (MEFxLMS) algorithm

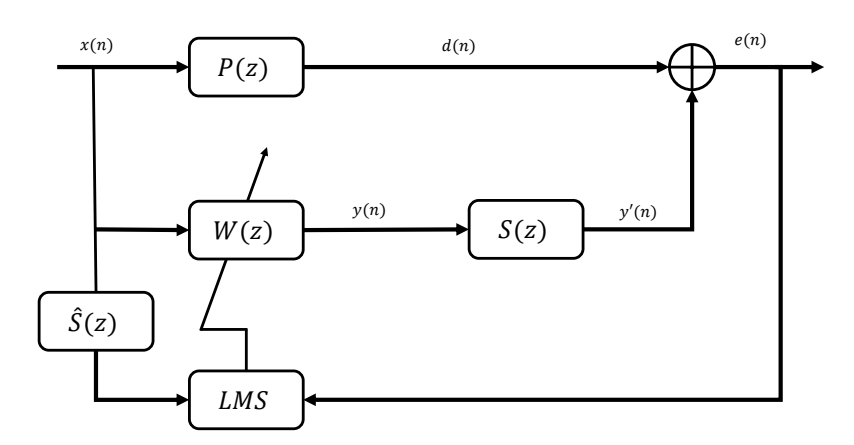


Figure 2.4: FxLMS for a broadband feedforward system, where $\hat{S}(z)$ represents the estimated secondary path.

Consider a generic multichannel control system comprised of *I* reference signals, *J* secondary sources, and *K* error sensor. The MEFxLMS algorithm, as illustrated in Figure 2.4, needs to know all the acoustic channel responses since it is based on the filtered-x scheme. Therefore, the acoustic





channels that link each secondary source with each error sensor must be estimated in a previous stage. The estimated acoustic channel between jth source and kth sensor is denoted by $\hat{\mathbf{s}}_{jk}$, and \mathbf{w}_{ij} stands for the adaptive filter that links reference signal $x_i(n)$ with jth secondary source. The centralized controller recursively computes a solution for the $I \cdot J$ adaptive filters as follows

$$\mathbf{w}_{ij}(n) = \mathbf{w}_{ij}(n-1) - \mu \sum_{k=1}^{K} \mathbf{v}_{ijk}(n) e_k(n), \qquad (2.1)$$

where the $[L \times 1]$ vector $\mathbf{w}_{ij}(n)$ is used in Figure 2.4 to filter the *i*th reference signal and obtain the corresponding signal contribution to secondary source $y_i(n)$. Constant μ is the step-size parameter and $\mathbf{v}_{ijk}(n)$ denotes a $[L \times 1]$ vector obtained by filtering the ith reference signal $x_i(n)$ with the Mlength estimated acoustic channel $\hat{\mathbf{s}}_{ik}$:

$$\mathbf{v}_{ijk}(n) = \mathbf{X}_i(n)\hat{\mathbf{s}}_{ik}, \tag{2.2}$$

where $X_i(n)$ is a circularly arranged matrix of the last M + L samples of $x_i(n)$:

$$\mathbf{X}_{i}(n) = \begin{bmatrix} x_{i}(n) & x_{i}(n-1) & \cdots & x_{i}(n-M+1) \\ x_{i}(n-1) & x_{i}(n-2) & \cdots & x_{i}(n-M+2) \\ \vdots & \vdots & \cdots & \vdots \\ x_{i}(n-L+1) & x_{i}(n-L+2) & \cdots & x_{i}(n-(L+M)+2) \end{bmatrix}.$$
(2.3)

Once the filter is calculated in Eq. (2.1), the j-th output signal that feeds the correspondent actuator is obtained as

$$y_j(n) = \sum_{I=1}^{I} \mathbf{w}_{ij}^T(n) [\mathbf{X}_i(n)]_{(:,1)},$$
(2.4)

where $[\mathbf{X}_i(n)]_{(:,1)}$ is the $[L \times 1]$ vector formed by the first column of $\mathbf{X}_i(n)$.

It should be noted that in Eq.(2.1) all the error signals $e_k(n)$ are necessary for the computation of each filter $\mathbf{w}_{ii}(n)$, hence the requirement of a centralized processor.

2.2.2 Other non-distributive control algorithms used in active casings

Various authors have developed and evaluated multi-channel implementations of these algorithms, as presented in [29, 30, 31] and [32]. Nevertheless, multi-channel FxLMS-based algorithms, such as those described in [33, 34], remain favored in certain applications due to their simplicity and ease of implementation. The tuning process becomes more complex as the system size increases, and the MEFxLMS algorithm becomes computationally demanding.

To mitigate this, one approach is to use only a single error signal at any given time, with designated intervals for switching between error sensors. The authors, in [28], declared this approach as Switched-Error FxLMS (SEFxLMS). The algorithm was tested on the active casing noise control model, exhibiting the same steady-state noise reduction as MEFxLMS algorithm. However, the slow adaptation rate of the SEFxLMS leads to a significant reduction in convergence rate as a trade-off to the reduced computational complexity. The Switched Multiple Error FxLMS (SMEFxLMS) is an extension to the SEFxLMS algorithm [35], it has a convergence rate and computational load between the performances of the SEFxLMS and the MEFxLMS. Figure 2.5 compares the performance of the MEFxLMS with SEFxLMS and SMEFxLMS reductions for simulations performed for a lightweight





casing at a 150 Hz tone disturbance. This system uses 21 actuator and 5 error microphone. Thus, the switching matrix is equal to:

$$\mathbf{G}_{L1} = \begin{bmatrix} 1 & 0 & 0 & 0 & 0 & 0 \\ 0 & 1 & 0 & 0 & 0 & 0 \\ 0 & 0 & 1 & 0 & 0 & 0 \\ 0 & 0 & 0 & 1 & 0 & 0 \\ 0 & 0 & 0 & 0 & 1 & 0 \\ 0 & 0 & 0 & 0 & 0 & 1 \end{bmatrix}$$

 G_{L1} uses the simplest variant with one active error microphone in this case.

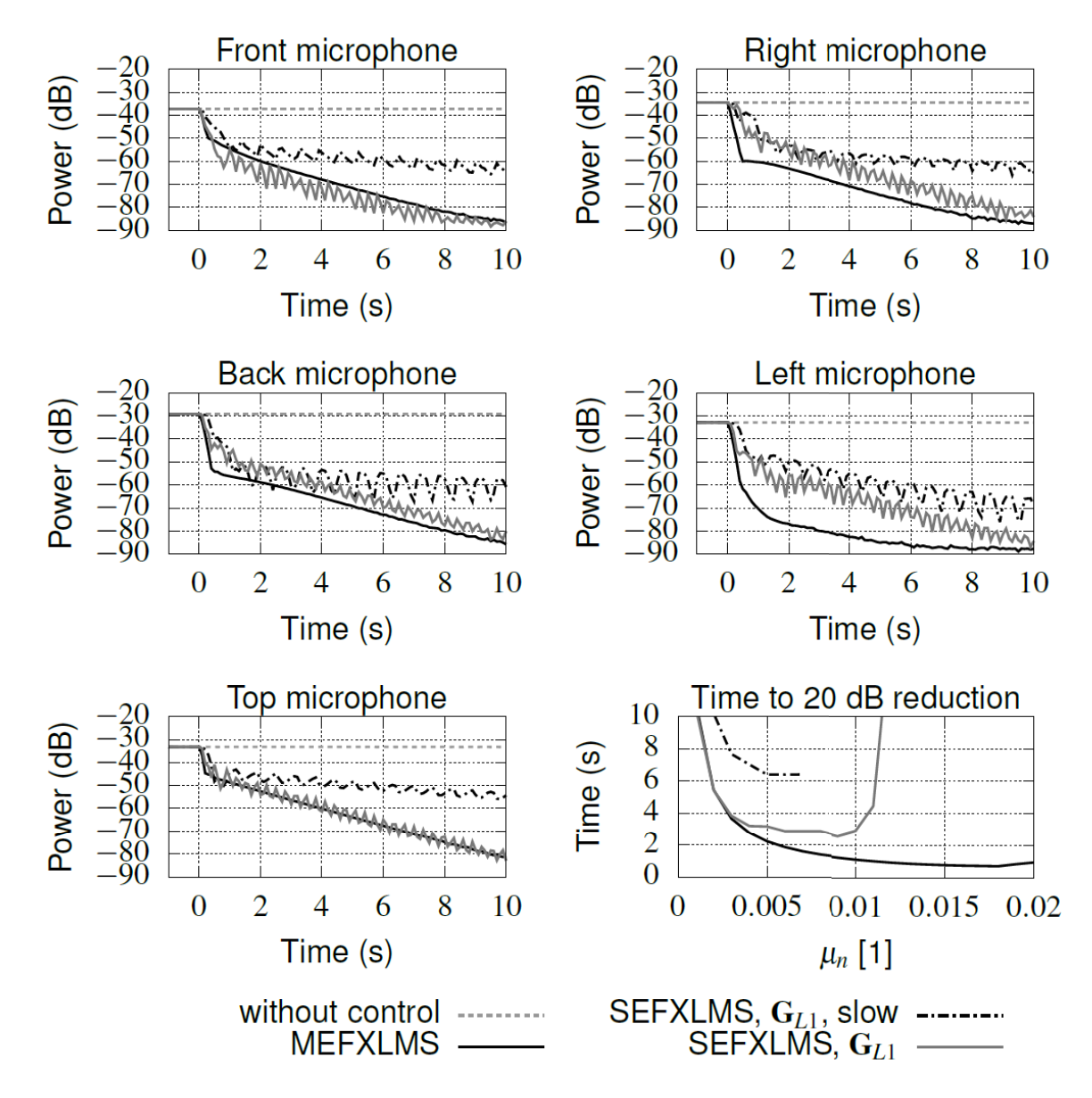


Figure 2.5: Error microphone signals power and time needed to obtain 20 dB noise reduction for different control algorithms (150 Hz tone, normalized step size $\mu_n = 0.005$, lightweight casing). Adapted from [36].

The "slow" variant refers to the case where, after switching errors, the adaptation process for N_S samples is disabled. In this case, filtered reference signals are calculated for at most N_Q error signals. To ensure proper control filter weight updates, N_S previously filtered reference signal samples are





required, and the filtered-reference filtering must be enabled in advance, before the error signal is activated.

The "slow" variant operates approximately 2 times slower than the SMEFxLMS, G_{L1} case due to the disabled adaptation phase. This comes at the expense of increased computational load, as it requires the calculation of higher number of the secondary paths associated with the next active error. Both variants are slower compared to the MEFxLMS algorithm. When convergence speed is a critical factor, the SMEFxLMS, G_{L1} variant is recommended. For a detailed description of the system and conclusion, refer to [36].

Chapter 3

A review of distributed algorithms for active control system

This chapter introduces the use of distributed algorithms in a typical multichannel ANC system. Section 3.1 provides a brief introduction to distribution networks, followed by an explanation of the classical Distributed MEFxLMS algorithm used in ANC systems in Section 3.2. Finally, a literature review of various other distributed algorithms is presented in Section 3.3.

3.1 Introduction of distributed networks

The concept of distributed networks in ANC systems is closely inspired by the capabilities and versatility of wireless sensor networks (WSNs), which have originally demonstrated their potential in decentralised systems across various applications. WSNs offer a cost-effective and scalable platform for implementing distributed control systems due to their ability to sense, process, and communicate data across spatially distributed nodes [37]. The potential of WSNs was evident from the beginning, with the proposal of various acoustic applications [38], leading to the development of specific wireless acoustic sensor networks (WASNs) whose sensor devices are microphones. These microphones are usually connected to a processor with communication and computation capability. Applications that make use of this kind of acoustic nodes are numerous and references therein, but they focus on the estimation of a standard signal or parameter that can be measured by all the nodes [39] or on the estimation of node-specific signals sharing some common properties or parameters [40]. Another typical feature of a node is related to its configuration: the acoustic node is usually composed of a microphone plus a processor, where the processing unit is dedicated to recording, control, and transmission tasks and can eventually perform some signal processing algorithms before transmission. However, this typical node structure needs to be modified in two aspects for applications involving sound control in general and particularly for active noise control (ANC) systems. First, the node should be able to act on the environment to control the sound rendering; that is, the node should be able to emit sounds through a loudspeaker or actuator. Second, the network should focus on estimating a particular signal or related parameter and designing the signals that will feed the loudspeakers and control the sound field. A generic acoustic node has a specific computation capability to process signals that can communicate to other nodes to exchange local and network status information and that are also able to act on their environment. The node can record signals through one or more mi-





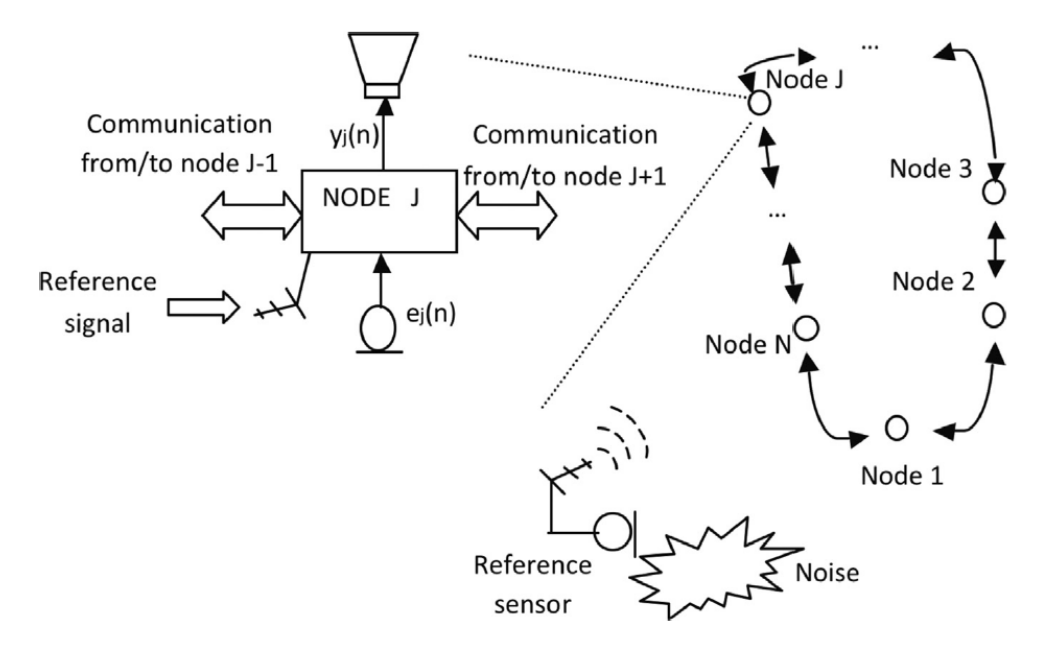


Figure 3.1: Single-channel acoustic node within a ring topology network. [41]

crophones (sensors) and emit sound signals via loudspeakers (actuators). In addition, nodes should use the network topology to process their signals properly. Some common topologies are the total diffusion networks, where all nodes are interconnected with the rest of the nodes; the mesh networks, where each node can communicate with a particular set of nodes; the tree networks, where communication between nodes is hierarchical; and the ring networks, where communication between nodes follows an incremental ordering along the network. Figure 3.1 shows a illustration of the schematic of an acoustic node within a ring topology network as an example.

3.2 Distributed MEFxLMS (DMEFxLMS) algorithm for ANC

Consider a generic multichannel control system comprised of I reference signals, J secondary sources and K error sensors. Also, a WASN of N single-channel nodes that will support an ANC system composed by N error sensors and N secondary sources. The objective of each node is to obtain its own adaptive filters such that they approach the minimization of global error but rely only on local data and some proper network information and distribute the computational burden among the different nodes.

Let us define a global $[ILN \times 1]$ filter vector $\mathbf{w}(n)$ as the ordered concatenation of all the filter vectors implemented at each node

$$\mathbf{w}(n) = \left[\mathbf{w}_1^T(n), \mathbf{w}_2^T(n), \dots, \mathbf{w}_N^T(n)\right]^T, \tag{3.1}$$

where $\mathbf{w}_k(n) = \begin{bmatrix} \mathbf{w}_{1k}^T(n), \mathbf{w}_{2k}^T(n), \dots, \mathbf{w}_{Ik}^T(n) \end{bmatrix}^T$ contains the IL filter coefficients that will be used at node k, and $\mathbf{w}_{ik}(n)$ was introduced in Eq. (2.1). Consequently we define the $[ILN \times 1]$ vector $\mathbf{v}_k(n)$ similar to $\mathbf{w}(n)$ in Eq. (3.1) as $\mathbf{v}_k(n) = \begin{bmatrix} \mathbf{v}_{1k}^T(n), \mathbf{v}_{2k}^T(n), \dots, \mathbf{v}_{Nk}^T(n) \end{bmatrix}^T$, where $\mathbf{v}_{jk}(n)$ denotes a $[IL \times 1]$ vector obtained





as

$$\mathbf{v}_{jk}(n) = \begin{bmatrix} \mathbf{v}_{1jk}(n) \\ \mathbf{v}_{2jk}(n) \\ \vdots \\ \mathbf{v}_{Ijk}(n) \end{bmatrix} = \begin{bmatrix} \mathbf{X}_{1}(n) \\ \mathbf{X}_{2}(n) \\ \vdots \\ \mathbf{X}_{I}(n) \end{bmatrix} \hat{\mathbf{s}}_{jk} = \mathbf{X}(n)\hat{\mathbf{s}}_{jk},$$
(3.2)

Matrix $\mathbf{X}(n)$ is the vertical concatenation of matrices $\mathbf{X}_i(n)$ defined as

$$\mathbf{X}_{i}(n) = \begin{bmatrix} x_{i}(n) & x_{i}(n-1) & \cdots & x_{i}(n-M+1) \\ x_{i}(n-1) & x_{i}(n-2) & \cdots & x_{i}(n-M+2) \\ \vdots & \vdots & \cdots & \vdots \\ x_{i}(n-L+1) & x_{i}(n-L+2) & \cdots & x_{i}(n-(L+M)+2) \end{bmatrix}.$$
(3.3)

which contain the last L + M samples of all the reference signals $x_i(n)$ properly arranged to perform the filtering.

Once the previous notation is stated, the filter updating equation in Eq. (2.1) can be extended to the whole network as

$$\mathbf{w}(n) = \mathbf{w}(n-1) - \mu \sum_{k=1}^{N} \mathbf{v}_k(n) e_k(n).$$
(3.4)

The main drawback of the distributed network is that each node has access only to its local data, $\{e_k(n), \mathbf{v}_k(n)\}$, thus each node can only calculate its own term in the sum of Eq. (3.4). Even for this only term, each node must know the secondary path estimates between all the secondary sources and its own error sensor, $\hat{\mathbf{s}}_{jk}$ for $1 \le j \le N$, but this requirement is not so critical since they can be estimated in a set-up stage.

To deal with a distributed processing, let us assume that the local updating is performed following an incremental strategy [39]: for a given time instant n, a complete round is performed along the network where each node computes its term of the summation in Eq. (3.4), aggregates it to the given filter vector and passes it to the following node in incremental order. To develop the formulation for this strategy, Eq. (3.4) is expressed as:

$$\mathbf{w}(n) = \mathbf{w}(n-1) - \mu \mathbf{v}_1(n)e_1(n) - \mu \mathbf{v}_2(n)e_2(n) - \dots - \mu \mathbf{v}_N(n)e_N(n). \tag{3.5}$$

Let us define the local version of the filter coefficient vector $\mathbf{w}(n)$ in node kth as

$$\mathbf{w}^{k}(n) = \begin{bmatrix} \mathbf{w}_{1}^{k}(n) \\ \mathbf{w}_{2}^{k}(n) \\ \vdots \\ \mathbf{w}_{N}^{k}(n) \end{bmatrix}, \tag{3.6}$$

and assume that at time n, node k = 1 has available the updated global vector obtained at time n - 1, such that $\mathbf{w}^1(n) = \mathbf{w}(n-1)$. Then at node k = 1 the following equation can be computed:

$$\mathbf{w}^{1}(n) = \mathbf{w}(n-1) - \mu \mathbf{v}_{1}(n)e_{1}(n). \tag{3.7}$$

Then, node 1 passes its local version of the filter vector to node k = 2 and this node updates its own local version as:

$$\mathbf{w}^{2}(n) = \mathbf{w}^{1}(n) - \mu \mathbf{v}_{2}(n)e_{2}(n),$$

Page 14 of 47 (3.8)



and so on till a whole round is done and at node k = N we obtain

$$\mathbf{w}^{N}(n) = \mathbf{w}^{N-1}(n) - \mu \mathbf{v}_{N}(n)e_{N}(n), \qquad (3.9)$$

which is equal to the expression of $\mathbf{w}(n)$ in Eq. (3.4), that is, the updated global filter can be as the local version of the vector at the last node $\mathbf{w}(n) = \mathbf{w}^N(n)$. Therefore, from Eq. (3.7)–(3.9), the general form of the filter updating at each node can be stated as

$$\mathbf{w}^{k}(n) = \mathbf{w}^{k-1}(n) - \mu \mathbf{v}_{k}(n)e_{k}(n), \ 1 \le k \le N,$$
(3.10)

assuming that the local version of the first node vector is given by $\mathbf{w}^0(n) = \mathbf{w}^N(n-1) = \mathbf{w}(n-1)$.

Finally, once the global updated vector at time instant n has been obtained as $\mathbf{w}(n) = \mathbf{w}^N(n)$, their values are disseminated to the rest of the nodes. Notice that only the local vector that corresponds to the IL coefficients from IL(k-1)+1 to ILk of $\mathbf{w}(n)$ defined as

$$\mathbf{w}_{k}(n) = [\mathbf{w}(n-1)]_{(IL(k-1)+1:ILk)}, \tag{3.11}$$

is needed to generate the *k*th node output signal $y_k(n)$:

$$y_k(n) = \mathbf{w}_k^T(n)[\mathbf{X}(n)]_{(:,1)},$$
 (3.12)

where $[\mathbf{X}(n)]_{(:,1)}$ is the $[IL \times 1]$ vector corresponding to the first column of $\mathbf{X}(n)$ defined in Eq. (3.2).

3.3 Other distributed algorithms used in ANC

The Multiple Error Filtered-x Least Mean Square (MEFxLMS) algorithm is formulated for WASNs as distributed MEFxLMS (DMEFxLMS), where adaptive filters are calculated and distributed over a ring topology with incremental communication. It cooperatively addresses the problem of linear estimation, in which nodes equipped with local computing abilities derive and share local estimates with their predefined neighbors. The computational burden is then shared among all processors [39]. In [16], they have extended DMEFxLMS to a network whose communication is affected by constant latency. To deal with this latency, the DMEFxLMS has been reformulated, introducing two new parameters: the first one acts in the meantime between two network information arrivals, deciding if the node adapts itself based on its local measurement or waits for the new network information. The second parameter only acts when the network information arrives at each node, providing different network and local information combinations. In [42], the filtered-x Least Mean Squares (FxLMS) strategy using a Frequency-domain Partitioned Block technique for the filtering operation (FPBFxLMS) is presented, which introduces collaboration between nodes following a diffusion strategy. This algorithm outperforms the non-collaborative strategy thanks to the network information exchanges among the nodes when the network nodes have a specific acoustic coupling between their acoustic channels.

The diffusion narrowband FxLMS (DNFxLMS), which is motivated by the practical advantages of acoustic sensor networks and narrowband FxLMS algorithm, is proposed to overcome the challenges of heavy computational load and system instability in the multichannel narrowband active noise control (MNANC) system in [43]. The DNFxLMS algorithm distributes the computational tasks among the individual nodes, reducing the computational load on a single controller.





The Augmented Diffusion FxLMS algorithm utilizes a neighborhood-based adaptation and node-based combination approach. In the adaptation phase, all the control filter weight vectors in the corresponding neighborhood of each node are collocated into an augmented vector, and the node processor estimates the augmented vector according to the error signal of the node. In the combination phase, the control filter weight vectors estimated by different neighbor nodes in the adaptation phase are averaged to update the node's control filter weights. The simulation results demonstrated that this algorithm is superior to Multitask Diffusion FxLMS (MDFxLMS), Decentralized FxLMS (DCFxLMS) in terms of either noise reduction, computational complexity, or stability. The DCFxLMS algorithm excels in noise reduction, computational complexity, and stability [44].

Affine projection algorithms have been shown to speed up the convergence speed of the algorithms. However, affine projection algorithms require matrix inversion, whose calculation is complex to distribute among the nodes. In [45], a distributed version of the affine-projection-like algorithm (which avoids matrix inversion) together with an incremental collaborative strategy in the network. It minimizes the power of the sum of the measured signals at the sensor locations over an acoustic sensor network (ASN), improving the LMS-type algorithms' convergence speed. In this model, every node can calculate a portion of the sum of the filter updating equation and supply the partial result to the next node to update the coefficients with their respective information. If this step is performed with an incremental strategy, the last node will have the updated coefficients. Finally, these coefficients are disseminated to the rest of the nodes to allow the system to generate the appropriate cancelation signals before the next iteration begins. However, the approximated versions of the multichannel filtered-x affine projection (MFxAP) can efficiently share the processing load among the nodes, but at the expense of worsening their convergence properties. In [46], the exact distributed multichannel filtered-x AP (EFxAP) The proposed algorithm obtains the same solution as the MFxAP algorithm as long as there are no communications constraints in the underlying ASN. In the EFxAP algorithm, each node can compute a part or the entire inverse matrix needed by the centralized MFxAP algorithm. A review summary of the distributed algorithm used is given in Table 3.3.1.





Table 3.3.1: Summary of the distributed algorithm used in active control system.

Summary							
Reference	Algorithm	Achivements					
[39]	Distributed MEFxLMS	It is distributed, cooperative, and able to respond in real-time to environmental changes.					
[16]	Distributed MEFxLMS	It exhibits the same performance as the centralized one when there are no communication constraints in the network.					
[42]	FPBFxLMS	It allows every node to update the global state of the network by using local information and assuming some collaboration with its neighbor nodes, as well. It obtains a good performance in contrast to the non-collaborative strategy because of the information of the network state calculated at each node spread all over the nodes.					
[43]	DNFxLMS	It enables the construction of NANC systems with a greater number of channels under the limitation of processor computing power.					
[44]	ADFxLMS	It has the same noise reduction performance as the centralized method even if the acoustic paths are strongly asymmetrical.					
[45]	DxAP	It exhibits faster convergence than the conventional least-mean-squares based algorithms as well as the same performance as its centralized version.					
[46]	EFxAP	It exhibits the fastest convergence and the highest noise level reduction for any size of the acoustic network and any projection order of the AP algorithm compared to the DMEFxLMS.					

Chapter 4

Virtual sensing techniques

This chapter explores the application of virtual sensing techniques in general ANC systems. While virtual sensing technique can aid the application of active casing by enabling effective control at a distance using structural sensors attached to the surface of the casing, or acoustic sensors located near the casing, its development has primarily been driven by other applications, in particular to local ANC. In many local ANC applications, such as the active headrest [47, 48, 49, 50, 51, 52, 53, 54], a spatially limited control zone can pose severe limitations in system performance. Moving the error microphones close to the position at which the sound field must be controlled is often not an option. To alleviate the problem, virtual sensing methods have been used to project control points away from physical microphones and closer to the location where sound field control is required. The concept is illustrated in Figure 4.1, where a virtual sensing method is used to move the control position closer to a listener's ear.

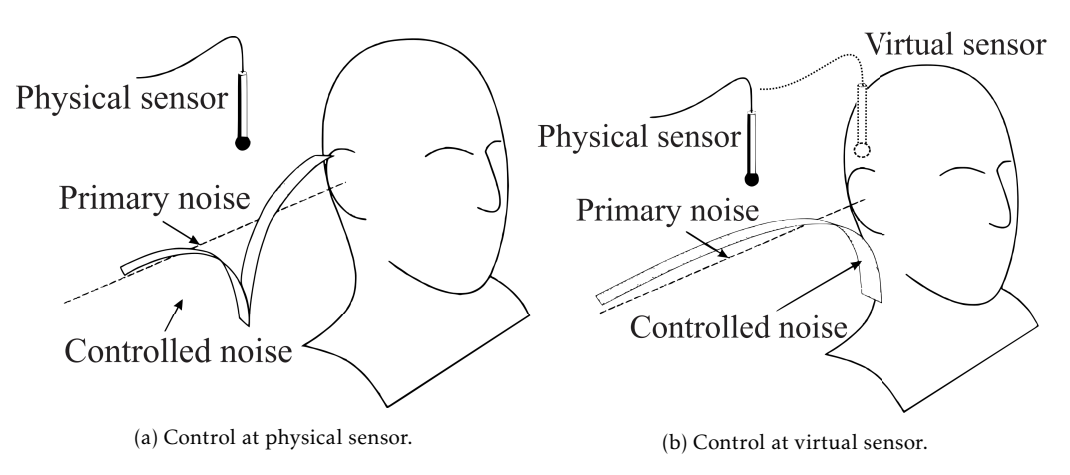


Figure 4.1: Local active noise control at the position of A) a physical sensor and B) a virtual sensor [55].

The possibility of moving the cancellation position to locations of interest away from physical sensors is very appealing and has motivated sustained research on virtual sensing techniques and their applications for more than thirty years [55, 56]. The virtual sensing problem can be described as the estimation of the sound field at the desired position, termed *virtual microphone*¹ from measurements with monitoring microphones at remote locations. The most prominent virtual sensing methods used in the context of ANC are presented next.

 $^{^1\}mathrm{This}$ corresponds to the error microphone in conventional ANC.





4.1 Virtual Microphone Arrangement

The *Virtual Microphone Arrangement* (VMA) is the first virtual sensing method used in the context of ANC, introduced by Elliott and David [55]. The block diagram of the method is shown in Figure 4.2. Assuming $N_{\rm m}$ monitoring and $N_{\rm e}$ virtual microphones and $N_{\rm u}$ secondary sources, the signals at the monitoring and virtual microphones are given by

$$m = d_{\rm m} + G_{\rm m}u \tag{4.1a}$$

$$e = d_e + G_e u, \tag{4.1b}$$

where $\mathbf{m} \in \mathbb{C}^{N_{\mathrm{m}}}$ and $\mathbf{e} \in \mathbb{C}^{N_{\mathrm{e}}}$ are the vectors of the monitoring and virtual microphone signals, $\mathbf{d}_{\mathrm{m}} \in \mathbb{C}^{N_{\mathrm{m}}}$ and $\mathbf{d}_{\mathrm{e}} \in \mathbb{C}^{N_{\mathrm{e}}}$ are the primary disturbances at the monitoring and virtual microphones, $\mathbf{u} \in \mathbb{C}^{N_{\mathrm{u}}}$ the driving signals for the secondary source, and $\mathbf{G}_{\mathrm{m}} \in \mathbb{C}^{N_{\mathrm{m}} \times N_{\mathrm{u}}}$ and $\mathbf{G}_{\mathrm{e}} \in \mathbb{C}^{N_{\mathrm{e}} \times N_{\mathrm{u}}}$ are the transfer function matrices from the secondary sources to the monitoring and virtual microphones, respectively. The task of the virtual sensing algorithm is to estimate the signals at the virtual microphones using the monitoring microphone signals. In the VMA, the disturbance field at the monitoring and virtual microphones is assumed to be equal, as shown in the block diagram, and the signals at the virtual microphone positions are given by

$$e = d_{e} - (\hat{G}_{m} - \hat{G}_{e})u, \tag{4.2}$$

with [:] denoting an estimated quantity.

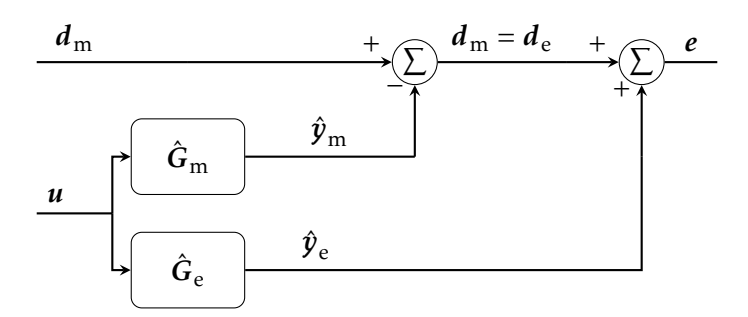


Figure 4.2: Block diagram of the Virtual Microphone Arrangement method [55].

During a preliminary *identification* (*tuning*, or *training*) stage, microphones are temporarily placed in the virtual positions and the transfer functions from the secondary sources to both the monitoring and virtual sensors are estimated. During the *control stage*, where the system is in operation, it is assumed that the primary disturbance at the virtual microphones is identical to that measured at the monitoring microphone locations and the secondary source signals are projected to the virtual microphone through the transfer function estimate \hat{G}_e .

The performance of the method has been investigated numerically and experimentally in head-rest applications [52, 53, 57]. It was shown that the controlled points can be effectively moved to the desired location, but the arrangement is sensitive to errors in the estimation of the primary disturbance at the virtual positions [57]. The estimation inaccuracies increase with frequency where the assumption of the primary sound field being equal at the physical and virtual microphone positions does not hold, and the performance of the method degrades. However, at low frequencies, good





stability and performance under perturbations of the plant responses were consistently reported [52, 53]. Horihata et al. [58] investigated the applicability of the method in locally controlling modal sound fields in enclosures. The spatial extent of the zones for which at least 10 dB of attenuation was attained, termed *Zones of Quiet* (ZoQ), was found to be comparable to that achieved when a physical microphone was used at the virtual microphone locations.

4.2 Remote Microphone Technique

The Remote Microphone Technique (RMT), introduced by Roure and Albarrazin, is an extension to the VMA [59]. To overcome the problem that the assumption of sound field equality introduces in the VMA, in this method the transfer function from the physical to the virtual microphones, termed observation filter, is estimated in the identification stage. During control, the filter is used to project the primary disturbance field to the virtual microphone positions. The block diagram of a purely feed-forward ANC system incorporating the RMT is shown in Figure 4.3, where the part enclosed in the dashed-line rectangle signifies the virtual sensing part.

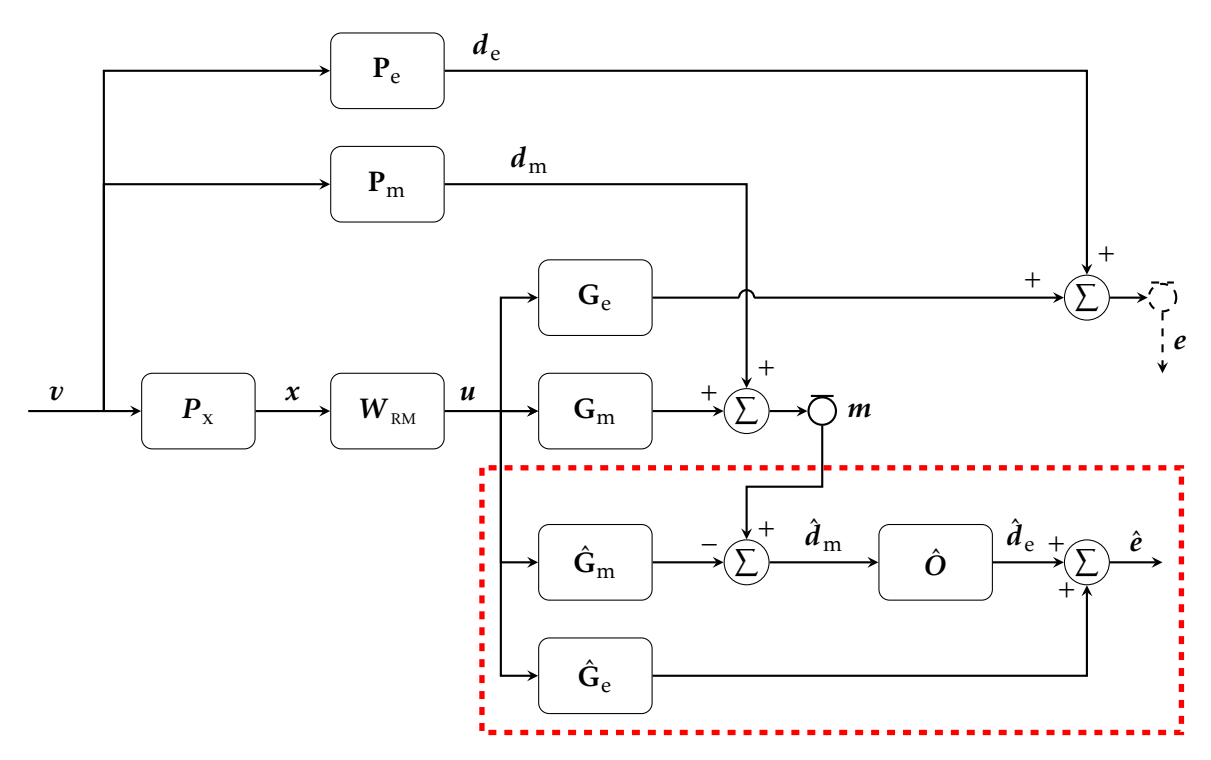


Figure 4.3: Block diagram of a purely feed-forward active control system with the remote microphone technique. The red dashed line signifies the virtual sensing part of the Remote Microphone Technique [48].

The vector v holds the complex strengths of N_v primary sources, which, through the transfer functions $P_x \in \mathbb{C}^{N_x \times N_v}$, $P_m \in \mathbb{C}^{N_m \times N_v}$ and $P_e \in \mathbb{C}^{N_e \times N_v}$, generate the disturbance field at the N_x , N_m and N_e reference, monitoring and virtual microphones respectively. In the absence of control, the true and estimated primary disturbance at the virtual microphones are

$$\hat{\boldsymbol{d}}_{e} = \hat{\boldsymbol{O}}\boldsymbol{d}_{m} = \hat{\boldsymbol{O}}\boldsymbol{P}_{m}\boldsymbol{v} \tag{4.3a}$$

$$d_e = P_e v, \tag{4.3b}$$



where \hat{O} is the observation filter that projects the measured monitoring microphone responses to the virtual microphone positions. Assuming that the source strengths are realisation of random processes, the optimal, in the least squares sense, observation filter can be calculated with a Wiener filtering approach [60], given by [61]

$$\hat{O}_{\text{opt}} = S_{\text{me}} (S_{\text{mm}} + \beta I)^{-1},$$
 (4.4)

where $[\cdot]^{-1}$ denotes matrix inversion, S_{mm} is the power-spectral density matrix of the monitoring microphone signals and S_{me} the cross-spectral density matrix between the monitoring and virtual microphone signals. I is an identity matrix of appropriate dimensions and β is a regularisation term discussed below.

During control, the observation filter is applied to the measured monitoring signals to acquire the estimate of d_e . Following the block diagram of Figure 4.3, the error at the virtual microphones is given by [61]

$$e - \hat{e} = P_{e}v + G_{e}u - \hat{O}_{opt}P_{m}v - \left[\hat{O}_{opt}\left(G_{m} - \hat{G}_{m}\right) + \hat{G}_{e}\right]u$$

$$= \left(P_{e} - \hat{O}_{opt}P_{m}\right)v - \left[\hat{O}_{opt}\left(G_{m} - \hat{G}_{m}\right) + \hat{G}_{e} - G_{e}\right]u.$$
(4.5)

It can be seen that if the plant response estimates \hat{G}_{m} and \hat{G}_{e} are perfect, the performance of the system depends entirely on the observation filter \hat{O}_{opt} through the first term in *equation* (4.5). An important drawback of the method is its susceptibility to uncertainties in the transfer functions from the primary and secondary sources to the monitoring microphones. Perturbations in P_{m} and errors in \hat{G}_{m} , can have a significant impact on the estimation performance since they are multiplied by the observation filter, including the inverse of a matrix, S_{mm} , which can often be ill-conditioned [62]. The regularisation term can be used to partially alleviate the problem [62], but this is done at the expense of decreased estimation accuracy [48].

The optimal filter that minimises the residual errors at the virtual microphone positions is calculated by minimising the squared error as given by *equation* (4.5) to get [62]

$$\hat{W}_{RM_{opt}} = -(G_{RM}^{H}G_{RM})^{-1}G_{RM}^{H}\hat{O}_{opt}S_{xm}S_{xx}^{-1},$$
(4.6)

where $G_{\text{RM}} = \hat{G}_{\text{e}} + \hat{O}_{\text{opt}} (G_{\text{m}} - \hat{G}_{\text{m}})$ and $[\cdot]^{\text{H}}$ denotes Hermitian transposition.

In a series of studies [54, 63, 64], the method has been augmented with head-tracking to allow for the estimation of moving points. Several observation filters and transfer functions were calculated and based on the position provided by the head tracker, the appropriate responses were used for control. Both performance and robustness showed significant improvement when compared to the static case, where the method can become unstable for large perturbations [65, 66].

Recently, a wave domain strategy utilising the RMT for noise control has been introduced [67, 68]. It has been demonstrated to be highly effective in controlling the sound field within a three-dimensional space, resulting in substantial sound reduction within a spherical radius of about 0.3 m. However, this approach requires a considerable number of microphones and loudspeakers, which may impede its practical implementation.







Misol [69] has effectively used the RMT in an ASAC application where the noise radiated by the sidewall panel in the interior of an aircraft fuselage was controlled at a varying number of virtual microphone positions. Mean attenuation of about 8 dB with peak values reaching 16 dB were recorded, however, the mean vibration levels of the panel were increased by up to 26 dB.

Virtual Microphone Control - Additional Filter 4.3

Pawełczyk [47] proposed the Virtual Microphone Control (VMC) to shift the control points to the desired locations. Other researchers have used the term Additional Filter (AF) method to refer to it [62] and this is adopted in this report. Like in the VMA and RMT, an initial tuning stage is required. During this phase, physical microphones are temporarily positioned at the virtual microphone locations and the primary disturbance is minimised there. When convergence has been achieved, filters modelling the transfer function between the monitoring and reference signals are estimated. The filters embed information on what the monitoring signals should be when the control algorithm has converged and constitutes the target response during control. The method has been found to be robust to uncertainties in the transfer responses from primary and secondary sources to the physical and virtual microphones with good performance even at frequencies up to 1 kHz [62, 65].

The block diagram of the method during the identification stage is shown in Figure 4.4. The filter $W_{\rm AF}$ is used to minimise the residual noise e at the virtual microphones. After convergence, the transfer function between the reference signals x, and the monitoring signals m is estimated through the filter \hat{H} . The estimate of the monitoring signals from those of the reference microphones when convergence of control has been achieved is given by [62]

$$\hat{\boldsymbol{m}} = \hat{\boldsymbol{H}}_{\text{opt}} \boldsymbol{x} \tag{4.7}$$

The optimal additional filter can be calculated following a Wiener filtering approach like the observation filter in the RMT and is given by [62]

$$\hat{H}_{\text{opt}} = \left(S_{\text{xm}} + \hat{G}_{\text{m}} \hat{W}_{\text{AF}_{\text{opt}}} S_{\text{xx}} \right) S_{\text{xx}}^{-1}, \tag{4.8}$$

where S_{xx} is the power spectral density matrix of the reference signals and S_{xm} is the cross-spectral density matrix between the reference and monitoring signals. $\hat{W}_{{}_{\mathrm{AF}_{\mathrm{opt}}}}$ is the optimal filter that minimises the residual noise at the virtual microphones during the identification stage and can be calculated in the optimal least-squares sense as [62]

$$\hat{W}_{AF_{opt}} = -\left(\hat{G}_{e}^{H}\hat{G}_{e}\right)^{-1}\hat{G}_{e}^{H}S_{xe}S_{xx}^{-1}.$$
(4.9)

The block diagram of the system during the control stage is shown in Figure 4.5. The sound reduction at the location of the virtual microphones is achieved by minimising the difference between the measured monitoring microphone signals and the monitoring signals when the residual noise at the virtual positions is minimised. The effective error signal is then given by [62]

$$\hat{\epsilon} = m - \hat{m} = m - \hat{H}_{\text{opt}} x = d_{\text{m}} + G_{\text{m}} W_{\text{AF}} x - \hat{H}_{\text{opt}} x = d_{\text{m}} + (G_{\text{m}} W_{\text{AF}} - \hat{H}_{\text{opt}}) x.$$
(4.10)
Page 22 of 47





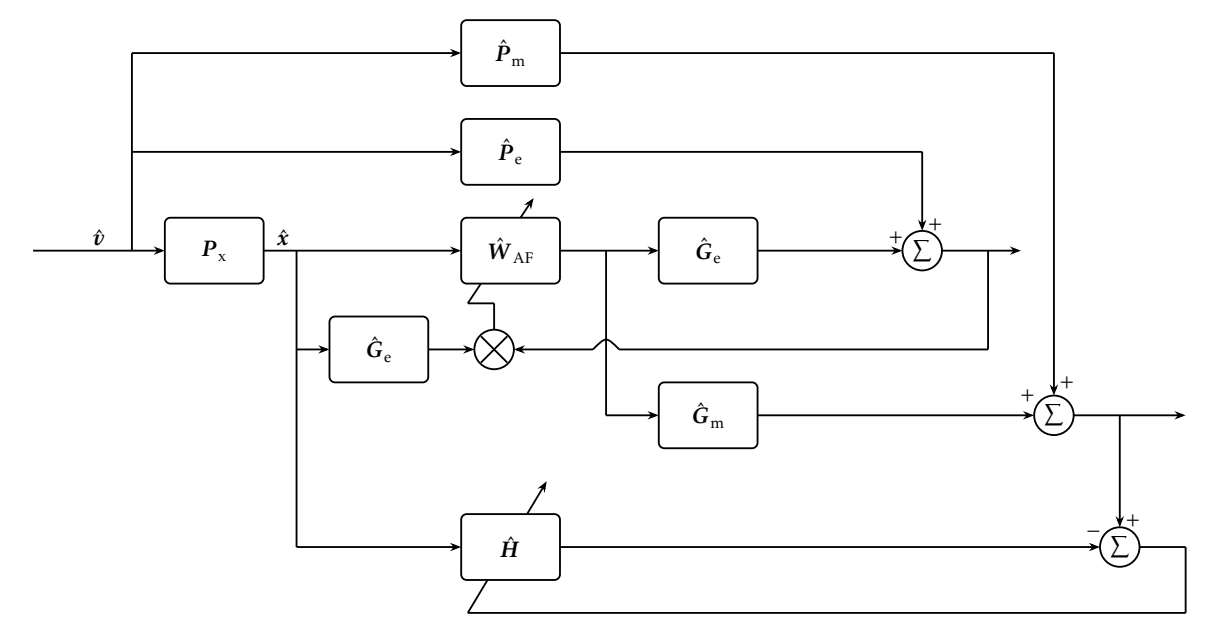


Figure 4.4: The block diagram of the Additional Filter method during the identification stage.

As can be seen in *equation* (4.10), the additional filter is used to minimise the differences between the measured monitoring signals and the estimate of these signals when the primary disturbance at the virtual microphones was optimally controlled. The optimal control filter is then calculated by the minimisation of the mean squared error of *equation* (4.10) to get [62]

$$W_{AF_{opt}} = (G_{m}^{H}G_{m})^{-1} G_{m}^{H} (\hat{H}_{opt}S_{xx} - S_{xm}) S_{xx}^{-1}.$$
 (4.11)

Since the error to be minimised is dependent on the reference signals as shown in *equation* (4.10), the method is sensitive to perturbations and uncertainties in the transfer functions from the sources to the reference sensors P_x [62, 65]. On the contrary, it can be seen that uncertainties in the plant responses or transfer functions from the primary sources to the virtual and monitoring sensors have minimal impact on the performance [62].

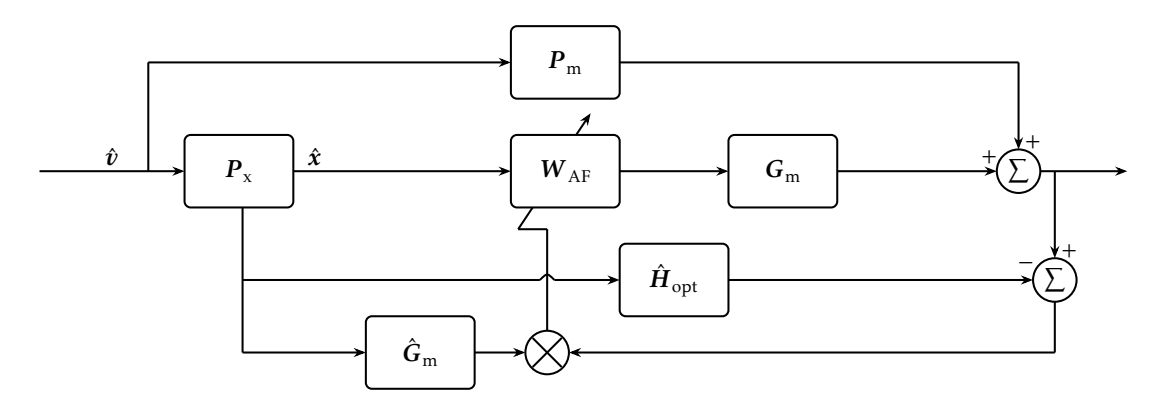


Figure 4.5: The block diagram of the Additional Filter method during the control stage.

To address the sensitivity of the method against perturbations in the reference signals, Shi et al. [70] introduced a variant that incorporates the training of multiple additional filters during the identification stage. In the control phase, a linear combination of additional filters is employed, chosen based on the frequency characteristics of the measured reference signals. This approach demonstrates





strated performance on par with conventional control at the virtual microphone position for both bandpass and wideband noise.

Similarly, Zhang et al. [71] proposed a method involving the training of multiple additional filters during the identification stage. In the control phase, the optimal filter is selected based on the minimisation of the energy at the virtual microphone position, which is estimated using an observation filter derived from a minimax optimisation process during identification. This method was evaluated in an active headrest system, showing significant improvements in performance and robustness compared to the RMT and AF methods for tonal and bandpass disturbances. However, the computational complexity of the method was found to be dependent upon the number of trained additional filters, resulting in a significantly higher complexity than both the RMT and AF.

Shi et al. [72] introduced the *Relative Path Virtual Sensing* (RP-VS) algorithm, which uses the control source signals measured to estimate the control signals at the virtual microphone positions through the use of a filter estimated during the training stage. The algorithm has been shown to behave similar to the RMT and AF methods under varying conditions of the acoustic transfer functions. The performance of the algorithm was validated in the context of an active-controlling casing further discussed in Chapter 5.

4.4 Kalman filtering

Petersen et al. [73] introduced a Kalman filtering formulation of an ANC system with embedded virtual sensing. The method, like the RMT and AF, requires an initial identification stage. The ANC system is modelled as a state-space system with outputs the monitoring and virtual microphone signals as [73]

$$z(n+1) = Az(n) + B_{\mathbf{u}}u(n) + B_{\mathbf{v}}v(n)$$
(4.12a)

$$e_{\rm m}(n) = C_{\rm m} z(n) + D_{\rm mu} u(n) + D_{\rm mv} v(n) + n_{\rm m}(n)$$
 (4.12b)

$$e_{e}(n) = C_{e}z(n) + D_{eu}u(n) + D_{ev}v(n) + n_{e}(n),$$
 (4.12c)

where z are the N plant states, $n_{\rm m}$ and $n_{\rm e}$ are the monitoring and virtual microphone noise signals, v are the $N_{\rm v}$ primary distrurbance signals and $e_{\rm m}$ and $e_{\rm e}$ are the $N_{\rm m}$ and $N_{\rm e}$ monitoring and virtual microphone signals respectively, with n denoting the discrete time index. In the state space model, $A \in \mathbb{R}^{N \times N}$ is the state space matrix, $B_{\rm u} \in \mathbb{R}^{N \times N_{\rm u}}$ and $B_{\rm v} \in \mathbb{R}^{N \times N_{\rm v}}$ are the secondary and primary input matrices and $C_{\rm m} \in \mathbb{R}^{N_{\rm m} \times N}$ and $C_{\rm e} \in \mathbb{R}^{N_{\rm e} \times N}$ are the monitoring and virtual output matrices. $D_{\rm mu} \in \mathbb{R}^{N_{\rm m} \times N_{\rm u}}$ and $D_{\rm mv} \in \mathbb{R}^{N_{\rm m} \times N_{\rm v}}$ are the monitoring feedforward matrices and $D_{\rm eu} \in \mathbb{R}^{N_{\rm e} \times N_{\rm u}}$ and $D_{\rm ev} \in \mathbb{R}^{N_{\rm e} \times N_{\rm v}}$ are the virtual feedforward matrices respectively. The noise terms $n_{\rm m}$ and $n_{\rm e}$ account for the noise at the monitoring and virtual microphones in the identification stage.

The primary signals and the monitoring and virtual noise signals are assumed to be realisations of white, zero mean random processes and their covariances are estimated at the initial identification stage. The virtual sensing algorithm that estimates the error signals at the virtual microphones is given by [55, 73]





$$\begin{bmatrix}
\hat{\boldsymbol{z}}(n+1|n) \\
\hat{\boldsymbol{e}}_{e}(n|n)
\end{bmatrix} = \begin{bmatrix}
\boldsymbol{A} - \boldsymbol{K}_{mv} \boldsymbol{C}_{m} & \boldsymbol{B}_{u} - \boldsymbol{K}_{mv} \boldsymbol{D}_{mu} & \boldsymbol{K}_{mv} \\
\boldsymbol{C}_{e} - \boldsymbol{M}_{ev} \boldsymbol{C}_{m} & \boldsymbol{D}_{eu} - \boldsymbol{M}_{ev} \boldsymbol{D}_{mu} & \boldsymbol{M}_{ev}
\end{bmatrix} \begin{bmatrix}
\hat{\boldsymbol{z}}(n|n-1) \\
\boldsymbol{u}(n) \\
\boldsymbol{e}_{m}(n)
\end{bmatrix},$$
(4.13)

with $K_{\rm mv}$ the Kalman gain matrix and $M_{\rm ev}$ the virtual innovation gain matrix, given by

$$\boldsymbol{K}_{\mathrm{mv}} = \left(\boldsymbol{A}\boldsymbol{P}_{\mathrm{mv}}\boldsymbol{C}_{\mathrm{m}}^{\mathrm{T}} + \bar{\boldsymbol{S}}_{\mathrm{mv}}\right)\boldsymbol{R}_{\mathrm{m}\varepsilon}^{-1} \tag{4.14a}$$

$$M_{\text{ev}} = (C_{\text{e}} P_{\text{mv}} C_{\text{m}}^{\text{T}} + \bar{R}_{\text{me}}^{-1}) R_{\text{m}\epsilon}^{-1}.$$
 (4.14b)

The symbol $[\cdot]^T$ denotes transposition, and the matrices \bar{S}_{mv} and \bar{R}_{me} are given by [55]

$$\bar{\mathbf{S}}_{\mathbf{m}\mathbf{v}} = \mathbf{D}_{\mathbf{m}\mathbf{v}}\mathbf{B}_{\mathbf{v}}^{\mathrm{T}} + \mathbf{S}_{\mathbf{m}\mathbf{v}}\mathbf{B}_{\mathbf{v}}^{\mathrm{T}} \tag{4.15a}$$

$$\bar{R}_{\text{me}} = R_{\text{me}}^{\text{T}} + S_{\text{mv}}^{\text{T}} D_{\text{ev}}^{\text{T}} + D_{\text{mv}} S_{\text{ev}} + D_{\text{mv}} D_{\text{ev}}^{\text{T}}$$
(4.15b)

where the matrices $S_{\rm mv}$ and $R_{\rm me}$ are the covariance matrices between the monitoring signals and the source and virtual signals and $S_{\rm ev}$ is the covariance matrix between the virtual and primary source signals and are given by [55, 73]

$$S_{\text{mv}} = E[\boldsymbol{n}_{\text{m}}(n)\boldsymbol{v}^{\text{T}}(k)]$$
(4.16a)

$$\mathbf{R}_{\text{me}} = \mathrm{E} \left[\mathbf{n}_{\text{m}}(n) \, \mathbf{n}_{\text{e}}^{\text{T}}(k) \right] \tag{4.16b}$$

$$S_{\text{ev}} = E[\boldsymbol{n}_{\text{e}}(n)\boldsymbol{v}^{\text{T}}(k)], \tag{4.16c}$$

where n and k are discrete-time indices and $E[\cdot]$ is the expectation operator. In equation (4.14) $\mathbf{R}_{m\epsilon}$ is the covariance matrix of the innovation signals $\epsilon_{m}(n) = \mathbf{e}_{m}(n) - \hat{\mathbf{e}}_{m}(n|n-1)$ and \mathbf{P}_{mv} is the unique solution to the Riccati equation and are given by [55]

$$P_{mv} = AP_{mv}A^{T} - (AP_{mv}C_{m}^{T} + \bar{S}_{mv})(C_{m}P_{mv}C_{m}^{T} + \bar{R}_{m})^{-1}(AP_{mv}C_{m}^{T} + \bar{S}_{mv})^{T} + Q_{v}$$
(4.17a)

$$\mathbf{R}_{\mathrm{m}\epsilon} = \left[\epsilon_{\mathrm{m}}(n)\,\epsilon_{\mathrm{m}}^{\mathrm{T}}(n)\right] = \mathbf{C}_{\mathrm{m}}\mathbf{P}_{\mathrm{mv}}\mathbf{C}_{\mathrm{m}}^{\mathrm{T}} + \bar{\mathbf{R}}_{\mathrm{m}},\tag{4.17b}$$

where $Q_v = B_v B_v^T$ is the covariance matrix of the process noise $w(n) = B_v v(n)$ and \bar{R}_m is the covariance matrix of the measurement monitoring microphone noise given by [55]

$$\bar{R}_{m} = R_{m} + S_{mv}^{T} D_{mv} + D_{mv} S_{mv} + D_{mv} D_{mv}^{T}, \tag{4.18}$$

with $R_{\rm m}$ being the covariance matrix of the monitoring microphone noise, equal to [73]

$$\mathbf{R}_{\mathrm{m}} = \mathrm{E} \left[\mathbf{n}_{\mathrm{m}}(n) \, \mathbf{n}_{\mathrm{m}}^{\mathrm{T}}(k) \right]. \tag{4.19}$$

In practice, the state space matrices and covariance matrices presented above need to be known to implement the Kalman filter. The preliminary identification stage is used to acquire the estimates Page 25 of 47





of the matrices and using subspace identification techniques a model in innovation form is estimated [55, 73]. In this form, the state space model of equation (4.12) becomes

$$\hat{\boldsymbol{z}}(n+1|n) = \hat{\boldsymbol{A}}\hat{\boldsymbol{z}}(n|n-1) + \hat{\boldsymbol{B}}_{\mathbf{u}}\boldsymbol{u}(n) + \hat{\boldsymbol{K}}_{\mathbf{v}} \left[\boldsymbol{\epsilon}_{\mathbf{m}}^{\mathsf{T}}\boldsymbol{\epsilon}_{\mathbf{e}}^{\mathsf{T}}\right]^{\mathsf{T}}$$
(4.20a)

$$\boldsymbol{e}_{\mathrm{m}}(n) = \hat{\boldsymbol{C}}_{\mathrm{m}}\hat{\boldsymbol{z}}(n|n-1) + \hat{\boldsymbol{D}}_{\mathrm{mu}}\boldsymbol{u}(n) + \boldsymbol{\epsilon}_{\mathrm{m}}(n)$$
(4.20b)

$$\boldsymbol{e}_{e}(n) = \hat{\boldsymbol{C}}_{e} \boldsymbol{z}(n|n-1) + \hat{\boldsymbol{D}}_{e1} \boldsymbol{u}(n) + \boldsymbol{\varepsilon}_{e}(n). \tag{4.20c}$$

The white innovation signals covariance matrix is then estimated as [55]

$$\hat{\mathbf{R}}_{\epsilon} = \begin{bmatrix} \hat{R}_{\mathrm{m}\epsilon} & \hat{R}_{\mathrm{m}\epsilon\epsilon} \\ \hat{R}_{\mathrm{m}\epsilon\epsilon}^{\mathrm{T}} & \hat{R}_{\mathrm{e}\epsilon} \end{bmatrix}. \tag{4.21}$$

Then, the Kalman filtering model is implemented as [55, 73]

$$\begin{bmatrix}
\hat{\boldsymbol{z}}(n+1|n) \\
\hat{\boldsymbol{e}}_{e}(n|n)
\end{bmatrix} = \begin{bmatrix}
\hat{\boldsymbol{A}} - \hat{\boldsymbol{K}}_{mv} \hat{\boldsymbol{C}}_{m} & \hat{\boldsymbol{B}}_{u} - \hat{\boldsymbol{K}}_{mv} \hat{\boldsymbol{D}}_{mu} & \hat{\boldsymbol{K}}_{mv} \\
\hat{\boldsymbol{C}}_{e} - \hat{\boldsymbol{M}}_{ev} \hat{\boldsymbol{C}}_{m} & \hat{\boldsymbol{D}}_{eu} - \hat{\boldsymbol{M}}_{ev} \hat{\boldsymbol{D}}_{mu} & \hat{\boldsymbol{M}}_{ev}
\end{bmatrix} \begin{bmatrix}
\hat{\boldsymbol{z}}(n|n-1) \\ \boldsymbol{u}(n) \\ \boldsymbol{e}_{m}(n)
\end{bmatrix},$$
(4.22)

where the Kalman gain and virtual innovation gain matrices \hat{K}_{mv} and \hat{M}_{ev} respectively are calculated as

$$\hat{\boldsymbol{K}}_{\text{mv}} = \left(\hat{\boldsymbol{A}}\hat{\boldsymbol{X}}_{\text{v}}\hat{\boldsymbol{C}}_{\text{m}}^{\text{T}} + \boldsymbol{K}_{\text{v}} \begin{bmatrix} \hat{\boldsymbol{R}}_{\text{me}} \\ \hat{\boldsymbol{R}}_{\text{me}}^{\text{T}} \end{bmatrix} \right) \left(\hat{\boldsymbol{C}}_{\text{m}}\hat{\boldsymbol{X}}_{\text{v}}\hat{\boldsymbol{C}}_{\text{m}}^{\text{T}} + \hat{\boldsymbol{R}}_{\text{me}} \right)^{-1}$$
(4.23a)

$$\hat{\boldsymbol{M}}_{\text{ev}} = \left(\hat{\boldsymbol{C}}_{\text{e}}\hat{\boldsymbol{X}}_{\text{v}}\hat{\boldsymbol{C}}_{\text{m}}^{\text{T}} + \hat{\boldsymbol{R}}_{\text{me}\varepsilon}^{\text{T}}\right) \left(\hat{\boldsymbol{C}}_{\text{m}}\hat{\boldsymbol{X}}_{\text{v}}\hat{\boldsymbol{C}}_{\text{m}}^{\text{T}} + \hat{\boldsymbol{R}}_{\text{m}\varepsilon}\right)^{-1}.$$
(4.23b)

In this model, the matrix X_v is the equivalent of P_{mv} in equation (4.17a) and is the unique solution to the discrete algebraic Ricatti equation given by [55]

$$\boldsymbol{X}_{v} = \hat{\boldsymbol{A}}\boldsymbol{X}_{v}\hat{\boldsymbol{A}}^{T} - \hat{\boldsymbol{K}}_{mv} \left(\hat{\boldsymbol{C}}_{m}\boldsymbol{X}_{v}\hat{\boldsymbol{C}}_{m}^{T} + \hat{\boldsymbol{R}}_{m\varepsilon}\right)^{-1} \hat{\boldsymbol{K}}_{mv}^{T} + \hat{\boldsymbol{K}}_{v}\hat{\boldsymbol{R}}_{\varepsilon}\hat{\boldsymbol{K}}_{v}^{T}. \tag{4.24}$$

When the noise covariance is known, the Kalman filter provides an optimal estimate of the virtual microphone error signals. This formulation accounts for measurement noise in both the monitoring and virtual microphone signals. However, its high computational complexity limits its practicality to relatively low-order models. Petersen et al. [73] compared this method to an FxLMS system for controlling random noise in a duct, achieving an overall broadband noise attenuation of approximately 19.7 dB at the virtual microphone's location, which is about 5.4 dB less than the conventional FxLMS method. Booij and Berkhoff [74] evaluated the Kalman filtering approach against the RMT in a "Silent Chair" system, where a broadband primary disturbance was controlled at two virtual positions near the chair's headrest. The RMT system outperformed the Kalman filter implementation due to the FIR filter's superior capability to estimate high-order models in greater detail than the state-space representation.





Halim et al. [75] designed a robust virtual sensing method based on the Kalman filter state space formulation for *Acoustic-Structural Active Control* (ASAC) of coupled enclosures. In a subsequent study, they calculated optimal positions for structural sensors based on the observability of the cavity modes [76]. Experimental results [77] revealed that the acoustic pressure was effectively reduced at frequencies around the modal frequencies of the cavity. The method and its performance are discussed in more detail in Chapter 5.

Chapter 5

Integration of virtual sensings and its distributed control algorithms in active casings

In the previous chapter, various distribution control algorithms and virtual sensing techniques were explored in ANC systems. Building on this foundation, this chapter outlines the implementation of distributed control and remote sensing strategies within the context of active casing. These strategies, developed in prior work, aim to enhance the system's performance and computation copmlexities by leveraging decentralised control and remote sensing methods.

5.1 Distributed control system implemented in active casings

Most ASAC systems commonly use centralized control architectures, in which a single processing unit manages the control processes for the entire network of sensors and actuators. Although effective for small-scale applications, centralized ASAC face challenges in scalability, real-time performance, and robustness to failures in large-scale or complex systems. Recent advancements have led to the integration of distributed control architectures [78] in ASAC applications[79, 80, 81], particularly for large-scale systems with spatially distributed sensors and actuators. These approaches aim to improve scalability while maintaining the stability of the control system. Figure 5.1 shows a comparison of decentralized, centralized, and distributed control architectures. In centralized architecture, a single controller is tasked with executing the control processes, whereas decentralized structures utilize multiple independent controllers for each channel. While similar to decentralized systems, distributed control architecture relies on collaboration among local controllers to preserve stability in complex, large-scale setups.

One notable contribution presented in [28] is the implementation of a distributed multichannel global ASAC system. The focus of this work is the development of a control framework that utilize multiple sensors and actuators to minimize vibro-acoustic emissions throughout the casing structure. Multiple dSPACE boards were used as a platform for the distributed ASAC system. Additionally, a faster variant of the distributed version of the SEFxLMS control algorithm was introduced in their framework which reduces the interaction between the boards. Fig.5.2 shows the global switching





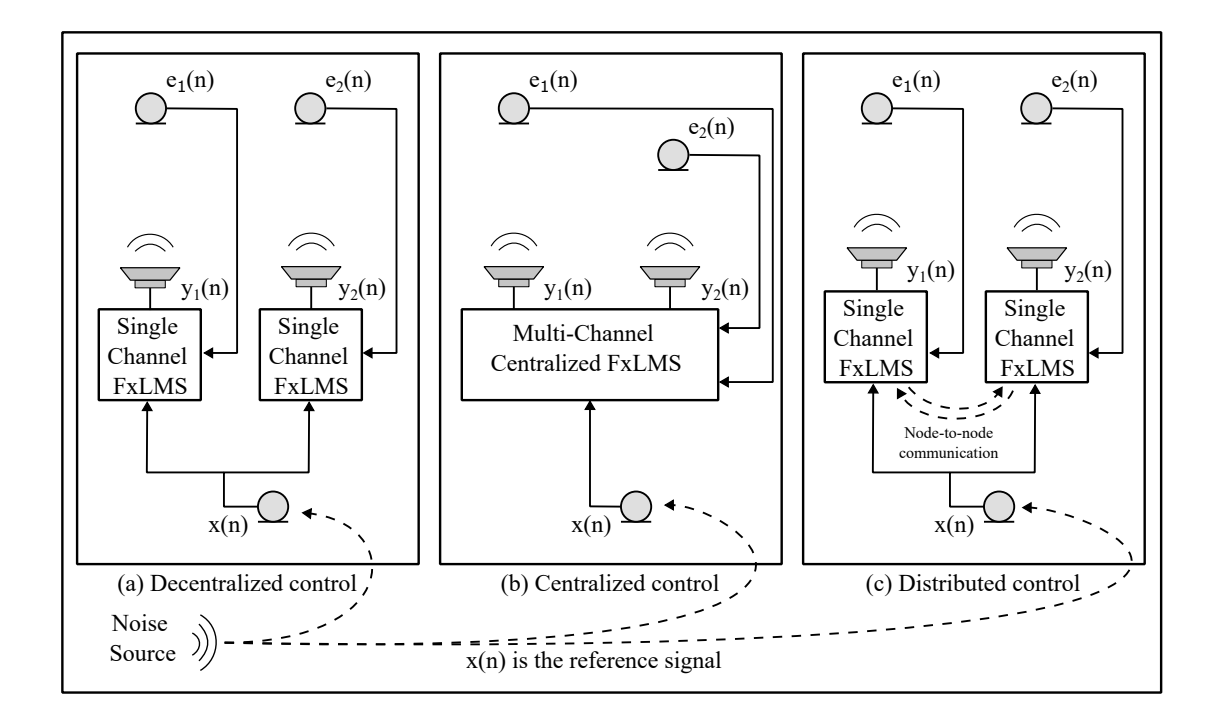


Figure 5.1: Schematic of decentralized, centralized and distributed architectures. The difference between (a) and (c) lies in the collaborative method used by the decentralized controllers.

scheme implemented for the distributed control algorithm. Given that the adaptation switch operates in a round-robin manner, filtering the reference signal prior to enabling adaptation for each controlled error signal is considered to be less efficient. Alternatively, enabling adaptation of the current error signal simultaneously with pre-filtering the reference signal for the next error signal enhances the convergence rate and eliminates a sample delay for the adaptation.

n	0 to $N_I - 1$	N_I to $2N_I - 1$	$2N_I$ to $3N_I - 1$	$3N_I$ to $4N_I - 1$	$4N_I$ to $5N_I - 1$	$5N_I$ to $6N_I - 1$	$6N_I$ to $7N_I - 1$	$7N_I$ to $8N_I - 1$	$8N_I$ to $9N_I - 1$	
s(n)	0	1	2	3	4	0	1	2	3	
e_0	+	1	1	1	FX	+	1	1	1	
e_1	FX	+	ı	ı	ı	FX	+	ı	ı	
e_2		FX	+	1	1	_	FX	+	ı	• • •
e_3	_	_	FX	+	_	_	_	FX	+	
e_4	_	_	_	FX	+	_	_	_	FX	

Figure 5.2: distributed SEFxLMS algorithm implemented for the noise-controlling casing. "+" refers to enabled adaptation, "FX" refers to Reference Filtering, "-" refers to disabled adaptation. Reused from [28]

Experimental results demonstrated that the distributed implementation achieved comparable noise reduction levels to the centralized approach while significantly reducing computational over-





head. In Fig. 5.3, the convergence performance of two Switched-error FXLMS variants is compared against the full MEFxLMS algorithm [33]. The SEFxLMS variants achieve the same steady-state attenuation as the original MEFxLMS. However, the MEFxLMS exhibits the highest convergence rate, followed by the faster SEFxLMS variant, and then the original SEFxLMS.

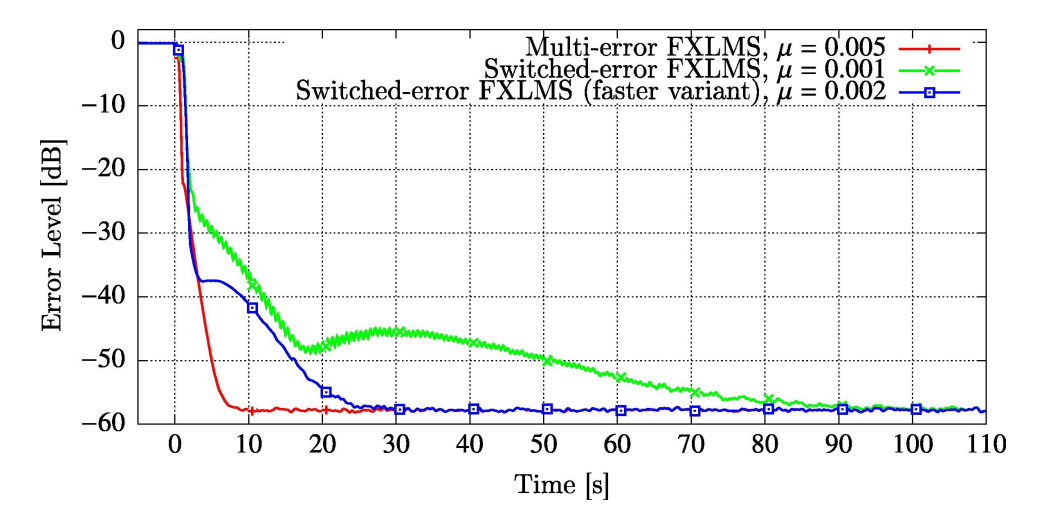


Figure 5.3: Comparison of performances of the SEFxLMS (old variant), SEFxLMS (faster variant) and the full MEFxLMS performed at 150 Hz tonal excitation. Reused from [28].

In [21], the same distributed architecture was used to control a real casing, referring to controlling the vibration of the panels of a washing machine in this context. The same architecture was used except that 4 dSPACE boards were used instead 5, due to the rear side of the washing machine positioned close to a wall. Fig 5.4 displays a photograph of the washing machine that was used for the experiment setup and it's dimensions.

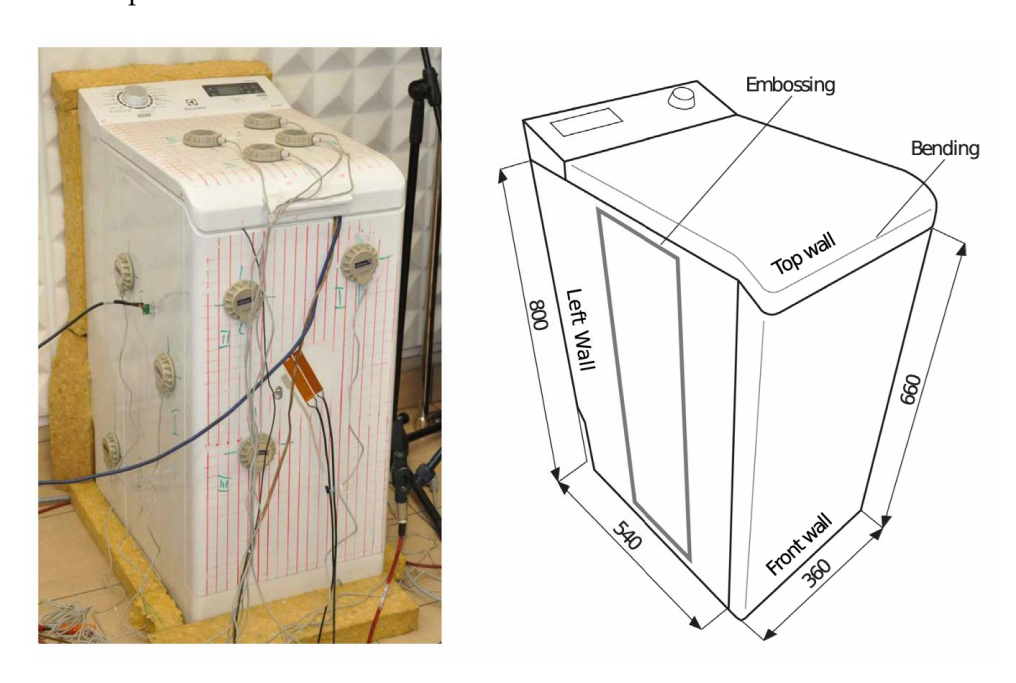


Figure 5.4: Photograph and dimensions of the washing machine casing. Dimensions are given in [mm]. Reused from [21].

.





The authors used the Leaky Normalized SEFxLMS algorithm as a control algorithm for each board. The authors also used Internal Model Control (IMC) control method for comparison between the performances. Table 5.1.1 shows the steady state reductions obtained for each error microphone positioned around the washing machine.

Table 5.1.1: SPL of the noise at the error microphones under two different control strategies (Feed-forward SEFxLMS Vs IMC). Reused from [21].

	Front [dB]	Right [dB]	Left [dB]	Top [dB]				
1200 rpm spinning								
Without control	73.2	79.1	79.7	72.9				
Feed-forward	63.8	69.8	67.0	65.1				
IMC	66.4	71.9	72.1	68.5				
113 Hz tonal dist	13 Hz tonal disturbance (6-th harmonic of the spinning noise)							
Without control	78.0	84.9	85.0	71.6				
Feed-forward	55.7	63.2	55.4	53.0				
IMC	53.9	62.5	55.0	53.6				

The average SPL reduction at the monitoring microphones for the feed-forward system is 7.4 dB (around 10 dB average reduction at error microphones), while for the IMC system, it is 4.7 dB (around 7 dB average reduction at error microphones) for the spinning noise. Global noise reduction can be achieved for tonal signals. Using 113 Hz as a tonal excitation for the noise, which corresponds to the 6th dominant harmonic of the spinning noise, the control system can provide attenuations that can exceed 13 dB on average using the SEFxLMS distributed setup and around 16 db on average using the IMC method. Thus, while the IMC method proves superior for tonal excitation, the distributed SEFxLMS configuration is better in attenuating harmonic disturbances.

5.2 Virtual Sensing Method for Active casing

This section presents the applications of VS in actively controlled casings, encompassing the three VS methods described in Chapter 4 along with their variants. Each VS system discussed utilises structural sensors to gather data, which is subsequently employed to estimate sound pressure at remote locations. The primary focus of the section is on describing the control performance of said methods, supplemented by additional information insights where relevant.

Remote Microphone-Based Virtual Sensing

The performance of the RMT has been investigated in the context of ASAC by Cheer and Daley [82] and was compared to the ability of an Active Vibration Control (AVC) in reducing the radiated noise of an enclosure, shown in Figure 5.5, excited at one of its resonances. The optimal and adaptively calculated control signals for the RMT-based ASAC and AVC systems were presented in closed form. 18 accelerometers were used to measure the structural response and 4 actuators were acting as secondary sources. At the initial identification stage, the acoustic and structural plant responses, G_p and G_s respectively, and the corresponding primary paths, P_p and P_s , were measured and the ob-





servation filters for 66 virtual microphone positions on a planar grid 0.07 m from the top side were calculated.

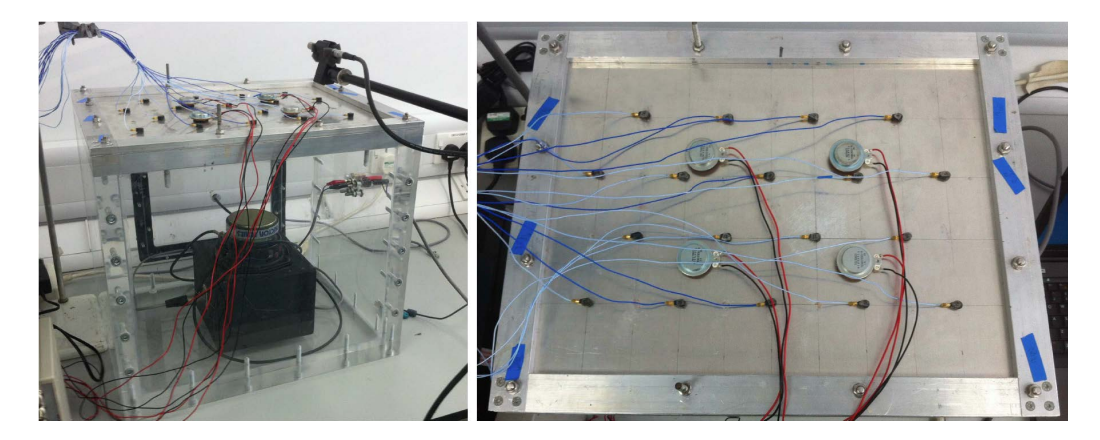


Figure 5.5: Enclosure used to evaluate the performance of an RMT-based ASAC system against an AVC [82].

The acoustic noise attenuation achieved by the RMT-based ASAC system is about 6 dB higher than that of the AVC as illustrated in 5.6 where the value of the cost function (sum of squared error signals) against time at the structural and acoustical sensors is shown. The ASAC achieves higher acoustic noise reduction because it controls the acoustic error signals directly, however, for the same reason, the vibration reduction is not as effective as that of the AVC [69]. The study demonstrates the applicability of the RMT method in ASAC applications. However, it is noted that due to the proximity of the virtual microphones to the casing far-field, global control is not guaranteed. It is suggested that using acoustic sensors at larger distances from the source could produce better results when it comes to global noise attenuation.

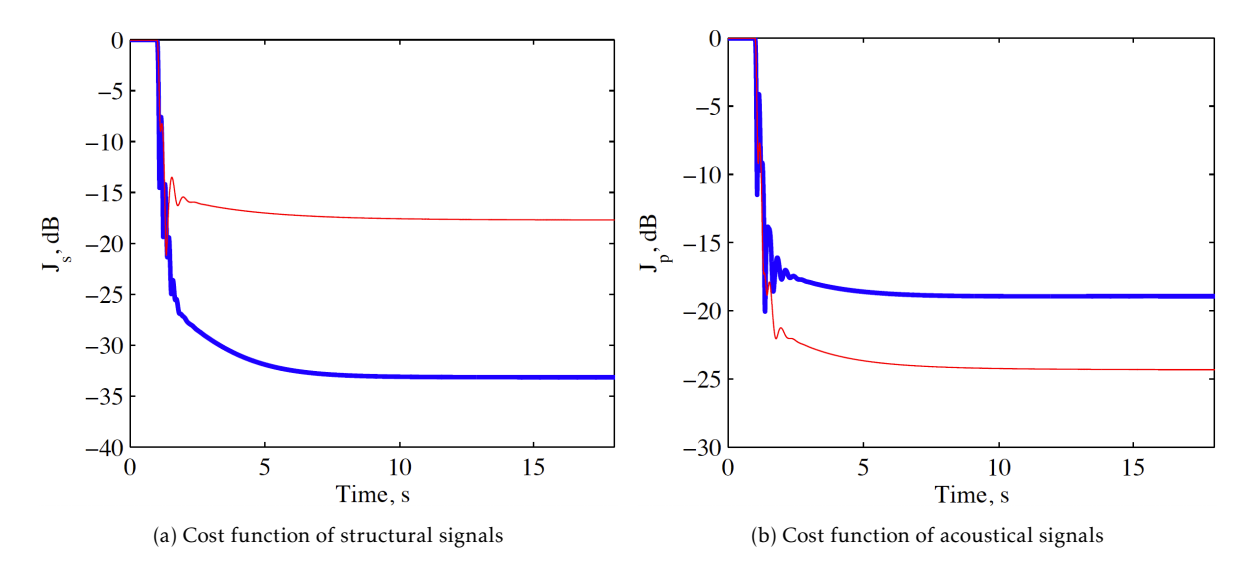


Figure 5.6: Convergence of the sum of squared error signals at the (a) structural and (b) acoustical sensors for the RMT-based (red) and AVC (blue) systems of Figure 5.5 [82].

Auxiliary Filter-Based Virtual Sensing (AF-VS)

In a similar experiment to that described in Section 5.2, Mazur and Pawełczyk [83], compared the performance of two ASAC systems, one with AF-based VS embedded and one of controlling the error signals at the virtual microphones by positioning physical microphones, to an AVC system. The three





methods were evaluated for an active-controlling casing shown in Figure 5.7a. One microphone is positioned at 0.5 m from each side of the casing to provide the error signals for the ANC system. On each panel of the casing three accelerometers were positioned to act as error signals for the AVC and three actuators, collocated with the accelerometers were used to control the vibrations for all deployed systems. The AF-based VS system uses the accelerometers as monitoring sensors and the microphones positions for the ANC system as error sensors. The global radiated noise reduction was evaluated at three microphones positioned far from the casing denoted as "M1" to "M3" in the schematic of Figure 5.7b.

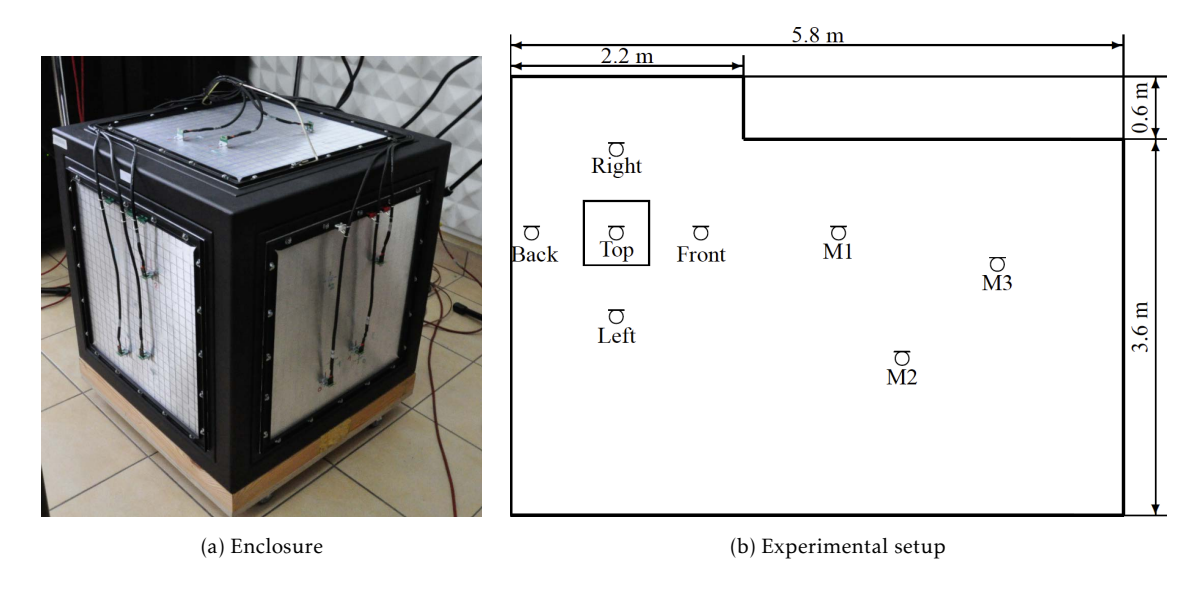


Figure 5.7: (a) Enclosure used to evaluate the performance of an AF-based ASAC system against an AVC and ANC system. (b) The schematic of the experimental setup; "Top", "Front", "Back", "Left" and "Right" denote the microphones used in the ANC and AF-based ASAC systems as error sensors and "M1", "M2" and "M3" are the microphones used to evaluate the global attenuation performance of the systems [83].

The systems were evaluated for tonal and multi-tonal disturbance signals of frequencies from 86 Hz to 196 Hz with a step of 2 Hz, reproduced by a loudspeaker positioned inside the casing. The spectrum of the signals in the microphones deployed in the far field, "M1", "M2" and "M3", during control are shown in Figure 5.8 for all three systems and the case of no control. The performance of the AVC system was found to be very poor with global attenuation being in the order of 1 dB. The best performance was observer with the ANC system with global noise reduction exceeding 10 dB and the AF-based system providing comparable results. However it should be noted that the AF-based system does not use microphones during the control phase and the required signals are acquired by the deployed accelerometers. In more detail, the amplitudes of all microphone signals are illustrated in Table 5.2.1 for the multi-tonal disturbance signal.

The Relative Path method and comparison with the Remote Microphone and Additional Filter methods

Shi et al. [72] introduce the RP-VS method briefly described in Section 4.2 and compared its performance against the RMT and AF methods in an active casing integrating an active feed-forward control system. Figure 5.9 illustrates the experimental setup, which consists of a variable-speed computer fan acting as the noise-emitting source enclosed within a casing designed to reduce noise while maintaining airflow for cooling purposes.





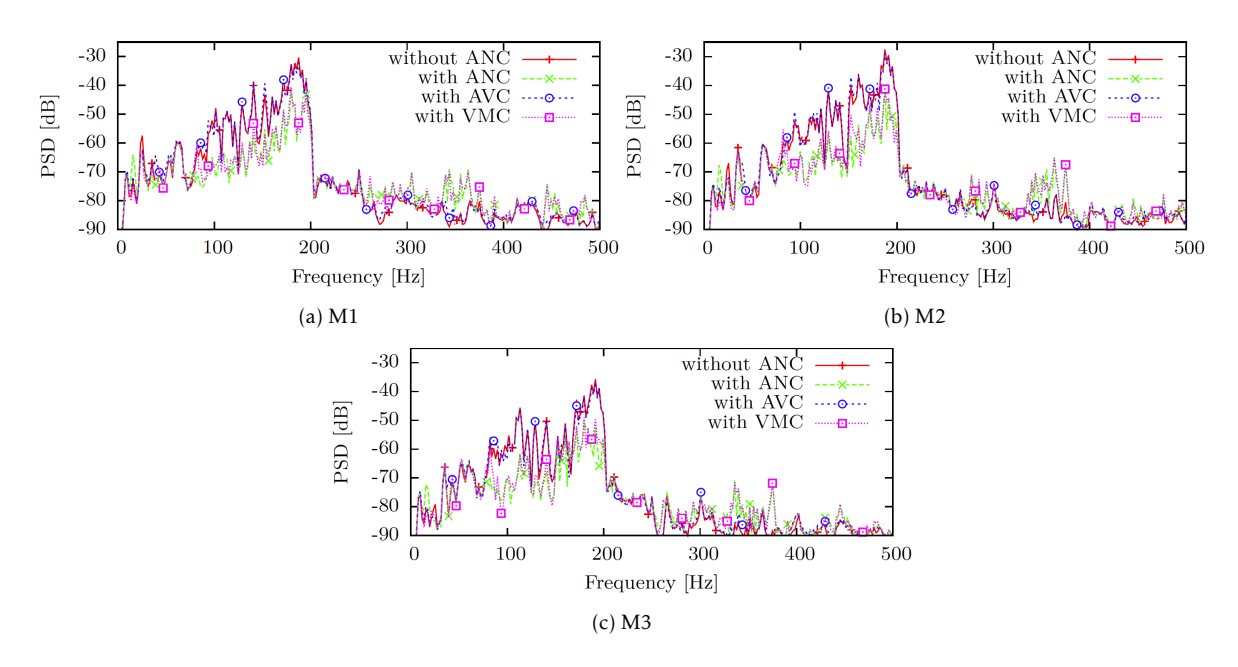


Figure 5.8: The signals at the far field microphones (a) M1, (b) M2 and (c) M3 without control and with control through the different control systems investigated in [83].

Table 5.2.1: Microphone signal amplitudes for a multitonal disturbance signal used for the evaluation of an AF-based ASAC, an AVC and and ANC system in [83]. The names of the microphones correspond to those presented in Figure 5.7b.

	Signal amplitude [dB]							
	Front	Right	Back	Left	Тор	M1	M2	M3
No control	-24.9	-19.5	-23.3	-24.1	-21.9	-20.7	-19.0	-26.4
ANC	-47.1	-46.1	-41.7	-41.6	-38.5	-32.9	-33.4	-39.2
AVC	-25.3	-20.2	-23.4	-24.6	-22.8	-21.5	-19.6	-27.2
VS-ASAC	-45.0	-42.8	-40.1	-40.6	-35.7	-31.7	-32.6	-38.1



The casing is equipped with multiple active control sources (loudspeakers), distributed near the openings to generate anti-noise waves. These waves counteract the noise emitted by the internal machinery, significantly reducing the sound pressure levels (SPL) in the target ZoQ. The setup also includes several monitoring microphones positioned around the casing to measure error signals, which are used to adaptively tune the control filters. The absence of physical microphones directly within the ZoQ is addressed by employing virtual sensing algorithms, namely the RMT, AF and RP methods, to estimate the error signals virtually.

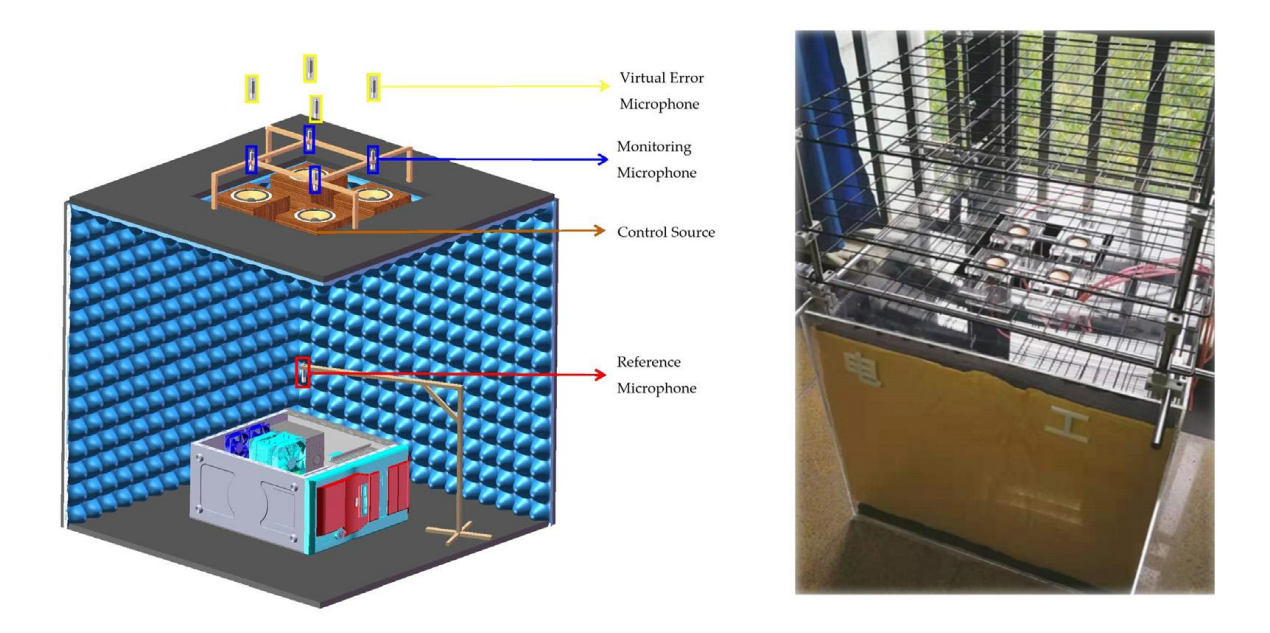


Figure 5.9: Schematic and picture of the experimental setup of the noise-cancelling casing, including the positions of the control sources, noise-emitting machinery, and monitoring microphones [72].

During the identification stage, the transfer functions between the sources and the reference, monitoring and virtual microphones, $P_{\rm x}$, $P_{\rm m}$ and $P_{\rm e}$ respectively and the plant responses $G_{\rm m}$ and $G_{\rm e}$, were estimated with the fan running at 30% of its full capacity. In the control stage, the fan was run at 30% and 100% of its maximum speed to evaluate the performance of the systems at variable operating conditions. The power spectra in the frequency range from 400 Hz to 1.6 kHz with the three VS systems and without control are illustrated in Figure 5.10 for both noise source conditions. The case of directly reducing the signals at the virtual microphones, denoted as FxLMS in the figure, is also shown and acts as a baseline, like in the study presented in [83].

When the conditions during control are identical to those used to "train" the systems, the performance of the AF method is very close to the FxLMS baseline system, and the other two VS systems provide comparable attenuation, as illustrated in Figure 5.10a. All three systems achieve significant attenuation at the virtual microphone locations over a wide spectrum up to frequencies exceeding 2 kHz. Figure 5.10b shows the spectra when the fan is running at its full workload. Under these conditions, all three methods continue to provide significant broadband noise reduction without retraining, but no method shows significant performance gains over the other two over the full bandwidth under consideration. This study demonstrates the suitability of the three VS methods for use in active casing systems, showcasing that they can effectively be used to reduce broadband noise at virtual microphone positions across varying source operational conditions, underscoring the methods' robustness in diverse, dynamic environments.



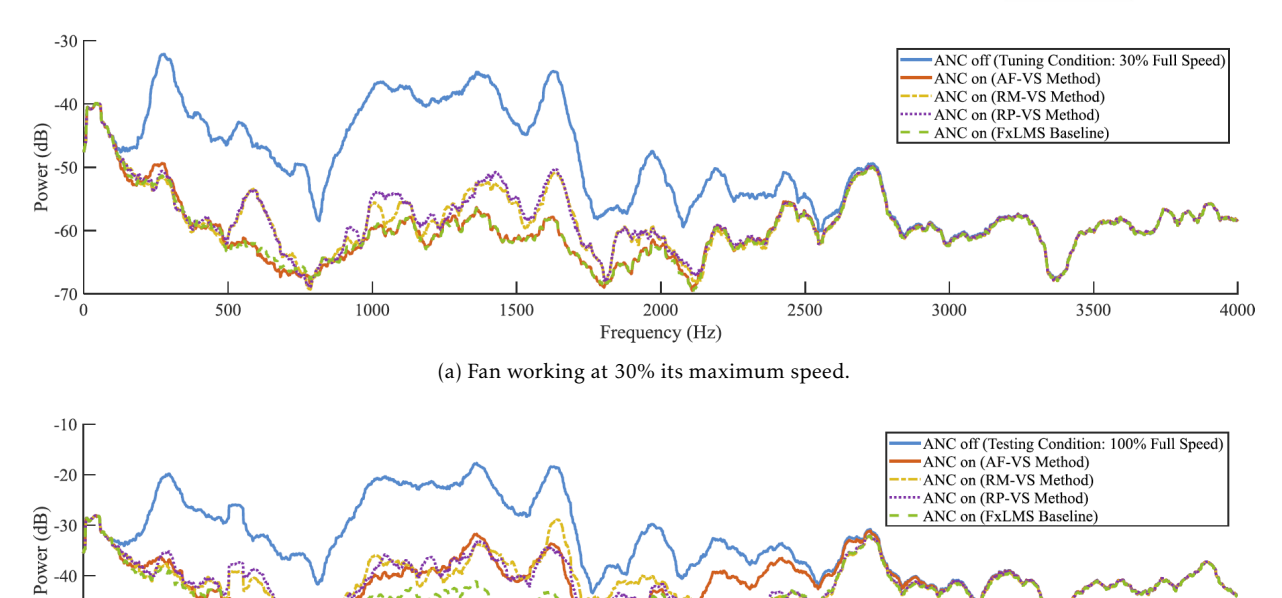
-50 -60

500

1000

Horizon Europe MSCA Doctoral Network IN-NOVA – Project no. 101073037





Frequency (Hz) (b) Fan working at 100% its maximum speed.

2000

2500

3000

3500

4000

Figure 5.10: Power spectra at the virtual microphones for the RMT, AF and RP methods when the fan acting as noise source is run at (a) 30% and (b) 100% of its maximum speed. The systems are "trained" with the fan running at 30% of its maximum speed [72].

Virtual microphone sensing through vibroacoustic modelling and Kalman filtering

1500

As described in [74] by Booij and Berkhoff and briefly discussed in Section 4.4, the Kalman filter can only be applied to low-order models due to its computational complexity. This was understood by van de Walle et al. [84], and they designed an ASAC system combining the Kalman filtering virtual microphone approach with a reduced-order (RO) finite-element model of a strongly coupled vibroacoustic casing shown in Figure 5.11a. The model was transformed into a first-order state-space representation and was introduced in the Kalman filtering formulation of the virtual sensing system. For the evaluation of the VS method the experimental setup illustrated in Figure 5.11b was used where a variable number of microphones denoted as "M1" to "M4" were used and the microphones "R1" and "R2" were used as reference microphones to evaluate the estimation performance. The system was excited with a modal hammer.

A system of 22993 Degrees-of-Freedom (DoF) was reduced to a model with only 68 DoFs, achieving a discrepancy between the two models smaller than about 2×10^{-5} across the spectrum spanning the frequencies from DC to 400 Hz. This model was employed in a Kalman filtering formulation to estimate the sound field within the casing, incorporating real-time sensor measurements. Figure 5.12 presents the estimated, measured and simulated pressure signals at the microphone "R2" from two distinct time intervals of approximately 0.15 s, starting at 0 s and 1 s. A strong agreement between the estimated and measured responses is demonstrated. However, while the simulations initially align well with the reference data, discrepancies arise over time due to error accumulation, leading to deviations from the actual pressure. It is important to note that the system was designed to ensure the long-term stability of the Kalman filter and due to the use of an RO model it allowed a numerically stable real-time implementation.





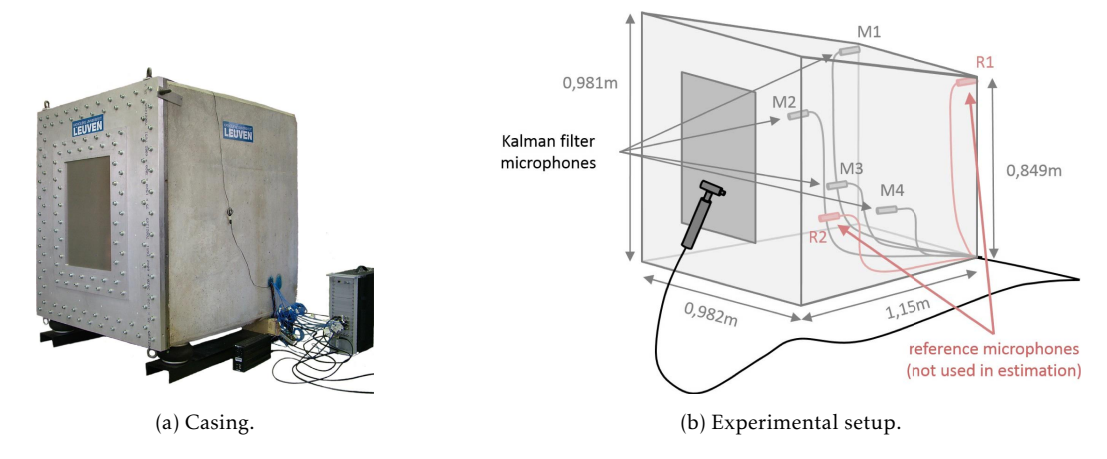


Figure 5.11: (a) The casing used to evaluate the performance of a Kalman filter VS used with a RO model of the casing, and (b) the experimental setup, where "M1" to "M4" are the monitoring microphones and "R1" and "R2" are reference microphones used to evaluate the performance of the system [84].

Halim et al. [75] designed an ASAC system incorporating virtual sensing through a Kalman filtering approach. A robust virtual sensing system was designed by optimally combining multiple Kalman sub-filters based on a minimax optimisation. The performance of the system was evaluated through numerical simulations of a modal vibroacoustic system with introduced uncertainties. The acoustic pressure generated by a volume velocity source inside the cavity of a casing was estimated with a single structural sensor. The pressure response controlled by a volume velocity source at a virtual sensor location inside the casing cavity is shown in Figure 5.13. The best and worst tonal active control performance is shown along with the uncontrolled pressure for comparison.

The performance of the virtual sensing system was found to be robust to uncertainties in the system. The ability of the system to sense the interior sound pressure at virtual microphone locations was demonstrated, and performance was shown to increase at frequencies corresponding to the modes of the cavity. Control performance was found to be dependent on the estimation accuracy, which in turn is critically dependent on the positioning of the structural sensor to achieve observability of a large number of modes. However, good control performance was achieved even at the worst-case dynamics corresponding to the highest uncertainty in the system.

In continuation of that research, the same authors investigated the optimal placement of structural sensors numerically to estimate the pressure field inside an acoustic-structural coupled enclosure accurately. The average output energy of the structural sensor generated by a spatially varying point source was used as the metric to optimise its position. The results of the study show that the metric is correlated with the observability of the cavity and panel modes in an additive manner. Importantly, it was demonstrated that to effectively detect a cavity mode, the structural sensor must be able to observe multiple structural modes that are strongly coupled to the acoustical mode. Taking into account both acoustical (cavity) and structural modes, an optimisation problem based on weighted observability of the modes, both structural and acoustical, was introduced to identify the optimal structural sensor position.

Halim and Cheng [77] experimentally investigated the work presented in [75, 76], focusing on active noise control within a casing. The study deployed loudspeakers as both primary and secondary sources, an accelerometer for structural measurements, and a microphone to measure pressure within the cavity. The experimental setup is illustrated in Figure 5.14. A Kalman filter virtual sensor was implemented following the methodology outlined in [75], and the FxLMS method was





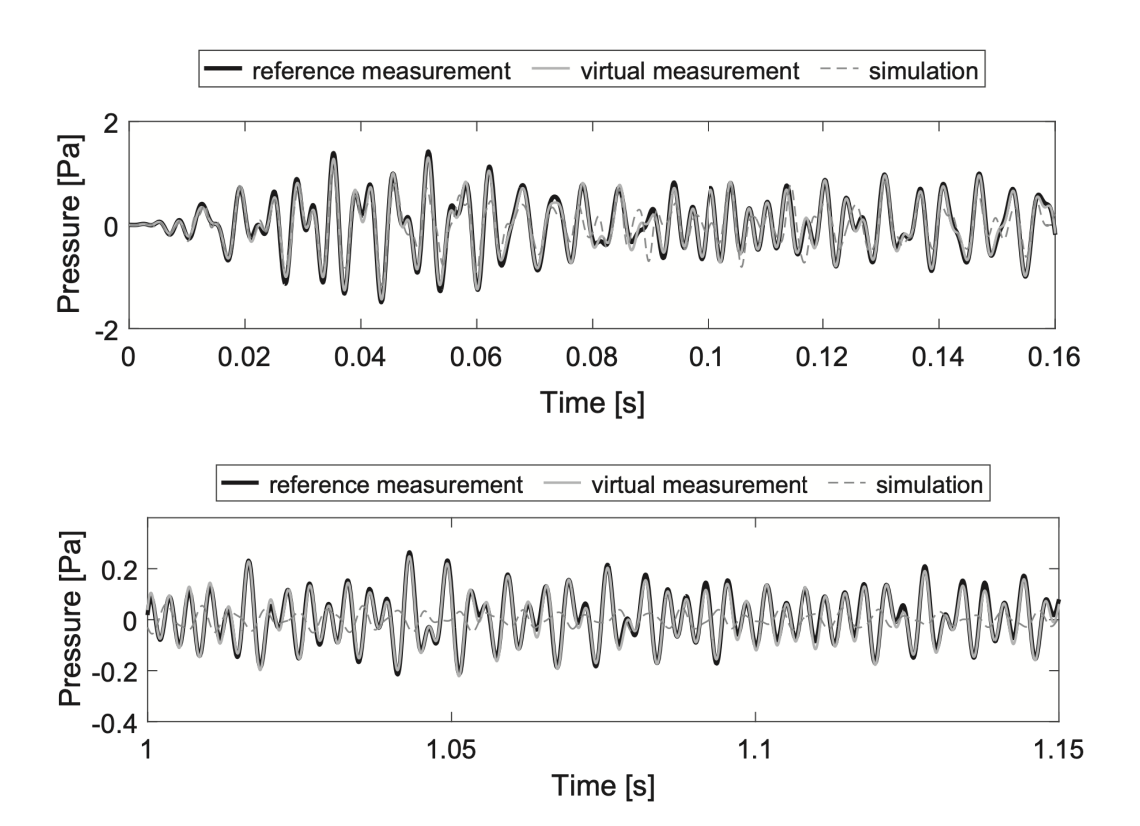


Figure 5.12: Measured, estimated and simulated pressure at the microphone position "R2" of Figure 5.11b at two time-spans of 0.15 s starting from 0 s and 1 s [84].

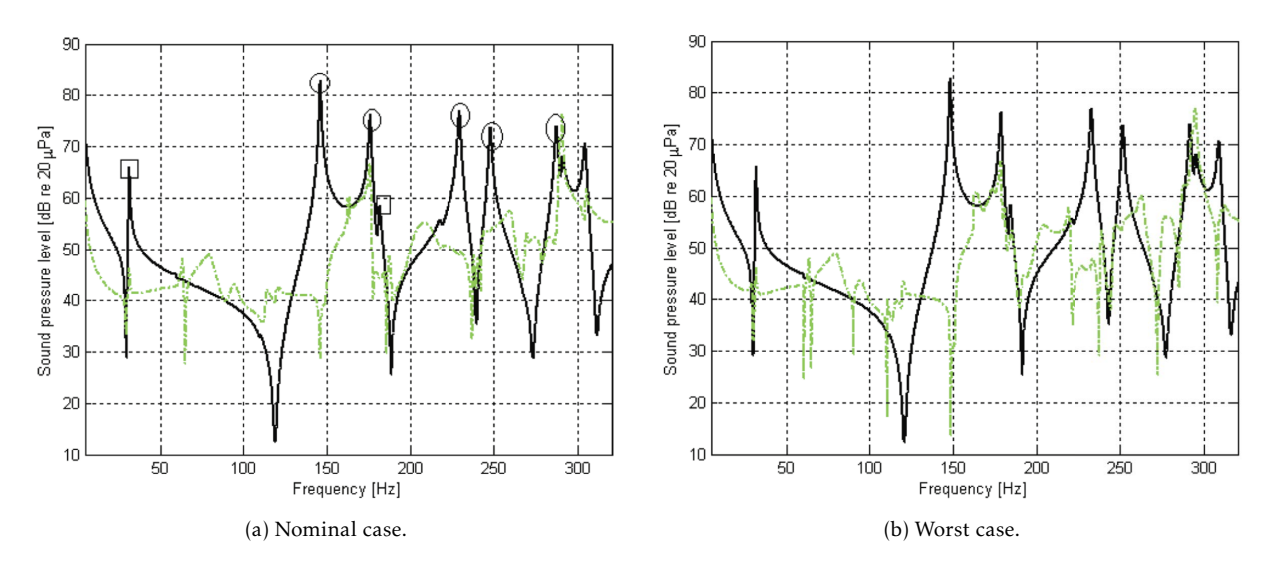


Figure 5.13: The (a) best and (b) worst pressure control performance inside a casing cavity achieved with a Kalman VS system. The solid line denotes (–) the primary disturbance and the dashed lines (- -) the actively controlled pressure for tonal excitation [75].





employed to realise the control system. The z dimension of the enclosure was variable to either 0.63 m or 0.64 m, and the upper clamps of the panel at which the accelerometer was attached could be removed; this allowed the investigation of the robustness of the system's performance under variable boundary conditions changing the dynamics of the panel.

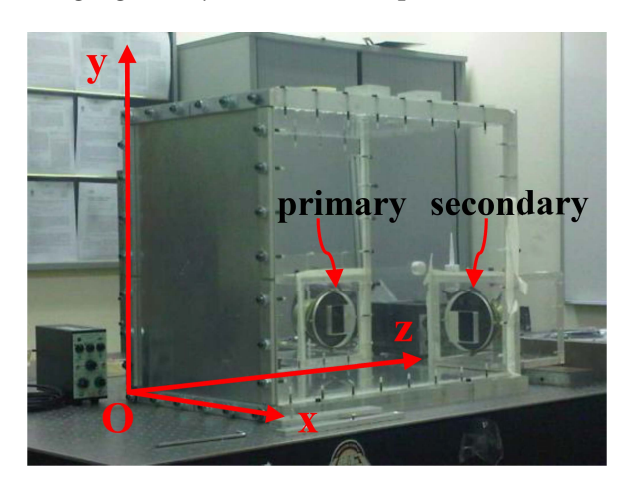


Figure 5.14: The experimental setup deployed in [77] to explore the performance of a Kalman filtering virtual sensor described in [75].

The objective was to achieve the highest possible attenuation under different conditions with a single Kalman filter implementation. The control performance under four different cases, one with the clamps and one without for each enclosure height, are depicted in Figure 5.15. It is demonstrated that the dominant modes are effectively sensed by the virtual sensor and controlled by the system under all conditions examined in the study. At some frequencies around 250 Hz, the acoustic pressure is slightly increased in all cases. However, the broadband sound pressure level is significantly reduced due to the controlled modes.

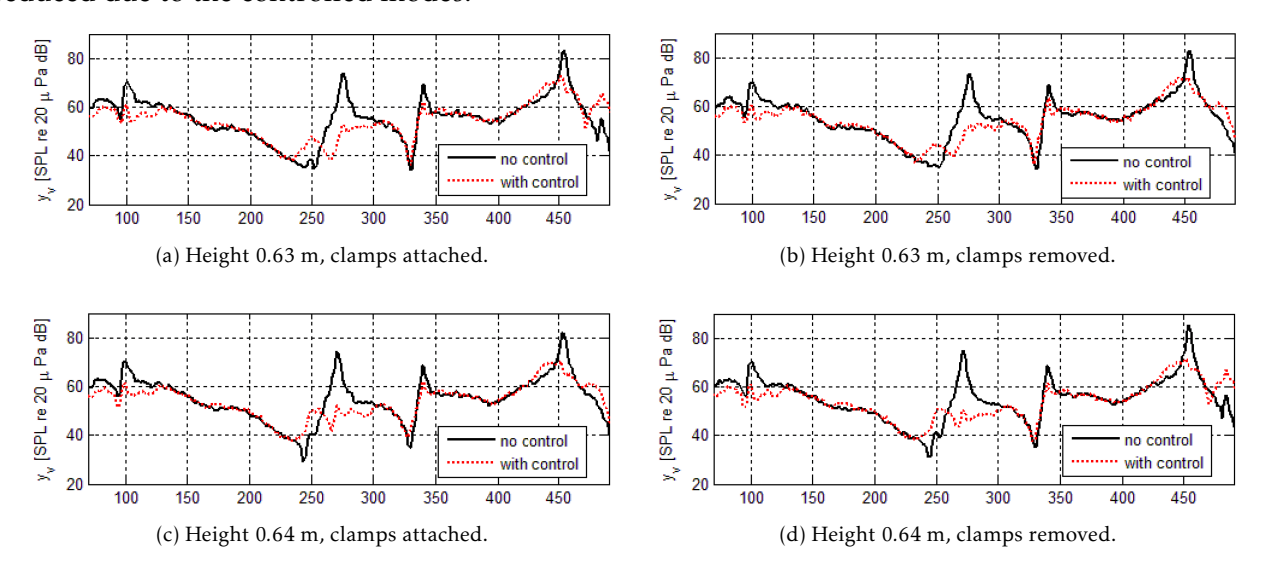


Figure 5.15: The sound pressure attenuation at a virtual microphone inside a casing achieved with a virtual sensing control system combining a Kalman filter virtual sensor and an FxLMS controller for four distinct cases [77].

Different approaches to using the Kalman filtering formulation to design a virtual sensor have been demonstrated above. In [84], a reduced-order finite element model was used to describe a vibroacoustic system in a state-space form and implement a virtual sensor. The combination of multi-





ple Kalman sub-filters was shown to provide a robust virtual sensor that was validated experimentally and through numerical simulations.

Chapter 6

Conclusion

While active control methods in casings show great potential for noise reduction, their effectiveness may still be limited by challenges such as computational complexity and physical design constraints. Although various approaches have been proposed to address computational complexity, such as sparse or decentralised algorithms, a trade-off between complexity and control performance often remains inevitable. Distributed algorithms offer a solution by mitigating this trade-off, as they improve control performance by distributing the workload across multiple processing units. These algorithms also facilitate communication between units, enabling a more coordinated and efficient control strategy. To overcome the physical design constraints imposed during the design process, virtual sensing techniques can be used to improve the noise control performance of the active casings.

This report investigates recent advancements aimed at addressing these challenges and highlights key innovations, such as distributed architectures and remote sensing techniques, that support the practical implementation of active control strategies. Although these techniques have been applied to active casing systems, as discussed in Chapter 5, further research is necessary to fully understand the limitations and constraints associated with these approaches. Understanding and addressing these constraints is important to realise the full capabilities of distributed control and remote sensing techniques for active casing applications.

Bibliography

- [1] European Environment Agency. Environmental noise in Europe, 2020. Technical report, Publications Office, 2020.
- [2] Marek Pawelczyk and Stanislaw Wrona. *Noise-Controlling Casings*. CRC Press, Boca Raton, 1 edition, June 2022.
- [3] Michael Möser. *Engineering Acoustics: An Introduction to Noise Control*. Springer Berlin Heidelberg, Berlin, Heidelberg, 2009.
- [4] Gülcan Aydın and Sait Eren San. Breaking the limits of acoustic science: A review of acoustic metamaterials. *Materials Science and Engineering: B*, 305:117384, July 2024.
- [5] Stephen Elliott. Signal Processing for Active Control. Academic Press, 2000.
- [6] P.A. Nelson, A.R.D. Curtis, S.J. Elliott, and A.J. Bullmore. The minimum power output of free field point sources and the active control of sound. *Journal of Sound and Vibration*, 116(3):397–414, August 1987.
- [7] Stephen J. Elliott, Jordan Cheer, Lam Bhan, Chuang Shi, and Woon Seng Gan. A wavenumber approach to analysing the active control of plane waves with arrays of secondary sources. *Journal of Sound and Vibration*, 419:405–419, 2018. Publisher: Elsevier Ltd.
- [8] Paul Leug. Process of silencing sound oscillations, June 1936.
- [9] Harry F. Olson and Everett G. May. Electronic Sound Absorber. *The Journal of the Acoustical Society of America*, 25(6):1130–1136, November 1953.
- [10] William B. Conover. Fighting Noise with Noise. Noise Control, 2(2):78-92, March 1956.
- [11] B. Widrow, J.R. Glover, J.M. McCool, J. Kaunitz, C.S. Williams, R.H. Hearn, J.R. Zeidler, Jr. Eugene Dong, and R.C. Goodlin. Adaptive noise cancelling: Principles and applications. *Proceedings of the IEEE*, 63(12):1692–1716, 1975.
- [12] Sakshi Gaur and V. K. Gupta. A Review on Filtered-X LMS Algorithm. *International Journal of Signal Processing Systems*, 4(2), 2015.
- [13] Dubravko Miljkovic. Active noise control: From analog to digital Last 80 years. In 2016 39th International Convention on Information and Communication Technology, Electronics and Microelectronics (MIPRO), pages 1151–1156, Opatija, Croatia, May 2016. IEEE.





- [14] Dongyuan Shi, Woon-Seng Gan, Bhan Lam, and Xiaoyi Shen. A Frequency-Domain Output-Constrained Active Noise Control Algorithm Based on an Intuitive Circulant Convolutional Penalty Factor. *IEEE/ACM Transactions on Audio, Speech, and Language Processing*, pages 1–14, 2023.
- [15] S.J. Elliott and C.C. Boucher. Interaction between multiple feedforward active control systems. *IEEE Transactions on Speech and Audio Processing*, 2(4):521–530, October 1994. Read_Status: Done Read Status Date: 2024-09-20T12:03:56.784Z.
- [16] Miguel Ferrer, Maria de Diego, Gema Piñero, and Alberto Gonzalez. Active noise control over adaptive distributed networks. *Signal Processing*, 107:82–95, 2015.
- [17] Danielle J. Moreau, Ben S. Cazzolato, and Anthony C. Zander. Active noise control at a moving location in a modally dense three-dimensional sound field using virtual sensing. *The Journal of the Acoustical Society of America*, 123(5_Supplement):3063–3063, May 2008.
- [18] Krzysztof Mazur and Marek Pawelczyk. Active control of noise emitted from a device casing. In *Proceedings of the 22nd International Congress of Sound and Vibration, Florence, Italy,* pages 12–16, 2015.
- [19] Krzysztof Mazur and Marek Pawelczyk. Internal model control for a light-weight active noise-reducing casing. *Archives of Acoustics*, 41(2), 2016.
- [20] Krzysztof Mazur and Marek Pawelczyk. Virtual microphone control for a light-weight active noise-reducing casing. In *Proceedings of 23th International Congress on Sound and Vibration*, volume 24, page 411284, 2016.
- [21] Krzysztof Mazur, Stanislaw Wrona, and Marek Pawelczyk. Active noise control for a washing machine. *Applied Acoustics*, 146:89–95, 2019.
- [22] Stanislaw Wrona and Marek Pawelczyk. Active reduction of device narrowband noise by controlling vibration of its casing based on structural sensors. In *Proceedings of the 22nd International Congress on Sound and Vibration, Florence, Italy*, pages 12–16, 2015.
- [23] Stanislaw Wrona and Marek Pawelczyk. Optimal placement of actuators for active structural acoustic control of a light-weight device casing. In *Proceedings of 23rd International Congress on Sound and Vibration, Athens, Greece*, pages 10–14, 2016.
- [24] S. Wrona, K. Mazur, M. Pawelczyk, and J. Klamka. Optimal placement of actuators for active control of a washing machine casing. In *Proceedings of 13th Conference on Active Noise and Vibration Control Methods*, 2017.
- [25] C. Fuller, M. McLoughlin, and S. Hildebrand. Active acoustic transmission loss box, April 28 1994.
- [26] Malte Misol, Stephan Algermissen, Michael Rose, and Hans Peter Monner. Aircraft lining panels with low-cost hardware for active noise reduction. In 2018 Joint Conference-Acoustics, pages 1–6. IEEE, 2018.
- [27] Joseph Milton, Jordan Cheer, and Steve Daley. Active structural acoustic control using an experimentally identified radiation resistance matrix. *The Journal of the Acoustical Society of America*, 147(3):1459–1468, 2020.





- [28] Krzysztof Mazur, Stanislaw Wrona, and Marek Pawelczyk. Design and implementation of multichannel global active structural acoustic control for a device casing. *Mechanical Systems and Signal Processing*, 98:877–889, 2018.
- [29] Martin Bouchard and Stephan Quednau. Multichannel recursive-least-square algorithms and fast-transversal-filter algorithms for active noise control and sound reproduction systems. *IEEE transactions on speech and audio processing*, 8(5):606–618, 2000.
- [30] Felix Albu, Martin Bouchard, and Yuriy Zakharov. Pseudo-affine projection algorithms for multichannel active noise control. *IEEE transactions on audio, speech, and language processing*, 15(3):1044–1052, 2007.
- [31] Ángel A Vázquez, Eduardo Pichardo, Juan G Avalos, Giovanny Sánchez, Hugo M Martínez, Juan C Sánchez, and Héctor M Pérez. Multichannel active noise control based on filtered-x affine projection-like and lms algorithms with switching filter selection. *Applied Sciences*, 9(21):4669, 2019.
- [32] María De Diego, Alberto Gonzalez, Miguel Ferrer, and Gema Pinero. An adaptive algorithms comparison for real multichannel active noise control. In 2004 12th European Signal Processing Conference, pages 925–928. IEEE, 2004.
- [33] S. Elliott, I. Stothers, and P. Nelson. A multiple error lms algorithm and its application to the active control of sound and vibration. *IEEE Transactions on Acoustics, Speech, and Signal Processing*, 35(10):1423–1434, 1987.
- [34] Scott C Douglas. Fast implementations of the filtered-x lms and lms algorithms for multichannel active noise control. *IEEE Transactions on speech and audio processing*, 7(4):454–465, 1999.
- [35] Krzysztof Mazur, Stanislaw Wrona, Anna Chraponska, Jaroslaw Rzepecki, and Marek Pawelczyk. Fxlms with multiple error switching for active noise-cancelling casings. *Archives of Acoustics*, 44(4):775 782, 2019.
- [36] M. Pawelczyk and S. Wrona. Noise-Controlling Casings. CRC Press, 2022.
- [37] Daniele Puccinelli and Martin Haenggi. Wireless sensor networks: applications and challenges of ubiquitous sensing. *IEEE Circuits and systems magazine*, 5(3):19–31, 2005.
- [38] Wei-Peng Chen, Jennifer C Hou, and Lui Sha. Dynamic clustering for acoustic target tracking in wireless sensor networks. *IEEE transactions on mobile computing*, 3(3):258–271, 2004.
- [39] Cassio G Lopes and Ali H Sayed. Incremental adaptive strategies over distributed networks. *IEEE transactions on signal processing*, 55(8):4064–4077, 2007.
- [40] Alexander Bertrand and Marc Moonen. Distributed adaptive node-specific signal estimation in fully connected sensor networks—part i: Sequential node updating. *IEEE Transactions on Signal Processing*, 58(10):5277–5291, 2010.
- [41] M. Ferrer, M. De Diego, G. Piñero, and A. Gonzalez. Active noise control over adaptive distributed networks. *Signal Processing*, 107:82–95, February 2015.
- [42] Christian Antoñanzas, Miguel Ferrer, Alberto Gonzalez, María de Diego, and Gema Piñero. Diffusion algorithm for active noise control in distributed networks. In *22nd International Congress on Sound and Vibration*, number July, 2015.





- [43] Jing Chen and Jun Yang. A distributed fxlms algorithm for narrowband active noise control and its convergence analysis. *Journal of Sound and Vibration*, 532:116986, 2022.
- [44] Tianyou Li, Siyuan Lian, Sipei Zhao, Jing Lu, and Ian S Burnett. Distributed active noise control based on an augmented diffusion fxlms algorithm. *IEEE/ACM Transactions on Audio, Speech, and Language Processing*, 31:1449–1463, 2023.
- [45] Christian Antoñanzas, Miguel Ferrer, Maria de Diego, and Alberto Gonzalez. Affine-projection-like algorithm for active noise control over distributed networks. In 2016 IEEE Sensor Array and Multichannel Signal Processing Workshop (SAM), pages 1–5. IEEE, 2016.
- [46] Miguel Ferrer, Maria de Diego, Gema Piñero, and Alberto Gonzalez. Affine projection algorithm over acoustic sensor networks for active noise control. *IEEE/ACM Transactions on Audio, Speech, and Language Processing*, 29:448–461, 2020.
- [47] Marek Pawelczyk. Adaptive noise control algorithms for active headrest system. *Control engineering practice*, 12(9):1101–1112, 2004.
- [48] Woomin Jung, Stephen J Elliott, and Jordan Cheer. Estimation of the pressure at a listener's ears in an active headrest system using the remote microphone technique. *The Journal of the Acoustical Society of America*, 143(5):2858–2869, 2018.
- [49] Harry F. Olson and Everett G. May. Electronic sound absorber. *Journal of the Acoustical Society of America*, 25:1130–1136, 11 1953.
- [50] P. S. Booij and A. P. Berkhoff. Virtual sensors for local, three dimensional, broadband multiple-channel active noise control and the effects on the quiet zones. In *Proceedings of ISMA 2010 International Conference on Noise and Vibration Engineering, including USD 2010*, pages 151–166. Katholieke Universiteit Leuven, 9 2010.
- [51] Jan Buck, Sergej Jukkert, and Delf Sachau. Performance evaluation of an active headrest considering non-stationary broadband disturbances and head movement. *The Journal of the Acoustical Society of America*, 143:2571–2579, 5 2018.
- [52] Marek Pawelczyk. Multiple input-multiple output adaptive feedback control strategies for the active headrest system: Design and real-time implementation. *International Journal of Adaptive Control and Signal Processing*, 17:785–800, 12 2003.
- [53] B. Rafaely, S. J. Elliott, and J. Garcia-Bonito. Broadband performance of an active headrest. *The Journal of the Acoustical Society of America*, 106:787–793, 8 1999.
- [54] Woomin Jung, Stephen J Elliott, and Jordan Cheer. Combining the remote microphone technique with head-tracking for local active sound control. *The Journal of the Acoustical Society of America*, 142:298–307, 2017.
- [55] Danielle Moreau, Ben Cazzolato, Anthony Zander, and Cornelis Petersen. A review of virtual sensing algorithms for active noise control. *Algorithms*, 1(2):69–99, 2008.
- [56] Lichuan Liu, Sen M Kuo, and MengChu Zhou. Virtual sensing techniques and their applications. In *IEEE International Conference on Networking, Sensing and Control*, pages 31–36. IEEE, 3 2009.





- [57] J Garcia-Bonito, SJ Elliott, and CC Boucher. Generation of zones of quiet using a virtual microphone arrangement. *The journal of the Acoustical Society of America*, 101(6):3498–3516, 1997.
- [58] S Horihata. Active noise control by means of virtual error microphone system. In *Proceedings INTER-NOISE97*, volume 529, 1997.
- [59] Alain Roure and Anne Albarrazin. The remote microphone technique for active noise control. In *Active 99*, pages 1233–1244. Institute of Noise Control Engineering, 1999.
- [60] Stephen Elliott. *Signal Processing for Active Control*. Signal Processing and its Applications. Academic Press, 1 edition, 2001.
- [61] Stephen J Elliott and Jordan Cheer. Modeling local active sound control with remote sensors in spatially random pressure fields. *The Journal of the acoustical Society of america*, 137(4):1936–1946, 2015.
- [62] Jin Zhang, Stephen J. Elliott, and Jordan Cheer. Robust performance of virtual sensing methods for active noise control. *Mechanical Systems and Signal Processing*, 152, 2021.
- [63] Stephen J Elliott, Woomin Jung, and Jordan Cheer. Head tracking extends local active control of broadband sound to higher frequencies. *Scientific reports*, 8(1):5403, 2018.
- [64] Stephen J Elliott, Jordan Cheer, and Woomin Jung. The effect of remote microphone technique and head-tracking on local active sound control. In 23rd International Congress on Sound & Vibration, 7 2016.
- [65] Stephen J. Elliott, Jin Zhang, Chung Kwan Lai, and Jordan Cheer. Superposition of the uncertainties in acoustic responses and the robust design of active control systems. *The Journal of the Acoustical Society of America*, 148:1415–1424, 9 2020.
- [66] Stephen Elliott, Chung Kwan Lai, Thibault Vergez, and Jordan Cheer. Robust stability and performance of local active control systems using virtual sensing. In *Proceedings of the International Congress on Acoustics*, volume 2019-September, 2019.
- [67] Huiyuan Sun, Jihui Zhang, Thushara D. Abhayapala, and Prasanga N. Samarasinghe. Active noise control over 3d space with remote microphone technique in the wave domain. In *IEEE Workshop on Applications of Signal Processing to Audio and Acoustics*, volume 2021-October, pages 301–305. IEEE, 10 2021.
- [68] Huiyuan Sun, Jihui Zhang, Thushara Abhayapala, and Prasanga Samarasinghe. Spatial active noise control with the remote microphone technique an approach with a moving higher order microphone. In *ICASSP*, *IEEE International Conference on Acoustics, Speech and Signal Processing Proceedings*, volume 2022-May, pages 8707–8711. Institute of Electrical and Electronics Engineers Inc., 2022.
- [69] Malte Misol. Active Sidewall Panels with Virtual Microphones for Aircraft Interior Noise Reduction. *Applied Sciences*, 10(19):6828, September 2020.
- [70] Chuang Shi, Rong Xie, Nan Jiang, Huiyong Li, and Yoshinobu Kajikawa. Selective Virtual Sensing Technique for Multi-channel Feedforward Active Noise Control Systems. In *ICASSP 2019 2019 IEEE International Conference on Acoustics, Speech and Signal Processing (ICASSP)*, pages 8489–8493, Brighton, United Kingdom, May 2019. IEEE.





- [71] Zeqiang Zhang, Ming Wu, Lan Yin, Chen Gong, Jun Yang, Yin Cao, and Lihua Yang. Robust parallel virtual sensing method for feedback active noise control in a headrest. *Mechanical Systems and Signal Processing*, 178:109293, 2022.
- [72] Chuang Shi, Zhuoying Jia, Rong Xie, and Huiyong Li. An active noise control casing using the multi-channel feedforward control system and the relative path based virtual sensing method. *Mechanical Systems and Signal Processing*, 144:106878, 2020.
- [73] Cornelis D. Petersen, Rufus Fraanje, Ben S. Cazzolato, Anthony C. Zander, and Colin H. Hansen. A Kalman filter approach to virtual sensing for active noise control. *Mechanical Systems and Signal Processing*, 22(2):490–508, February 2008.
- [74] P S Booij and A P Berkhoff. Virtual sensors for local, three dimensional, broadband multiple-channel active noise control and the effects on the quiet zones. In *ISMA 2010*, pages 151–166, Sharjah, United Arab Emirates, April 2010.
- [75] Dunant Halim, Li Cheng, and Zhongqing Su. Virtual sensors for active noise control in acoustic–structural coupled enclosures using structural sensing: Robust virtual sensor design. *The Journal of the Acoustical Society of America*, 129(3):1390–1399, March 2011.
- [76] Dunant Halim, Li Cheng, and Zhongqing Su. Virtual sensors for active noise control in acoustic-structural coupled enclosures using structural sensing: Part II—Optimization of structural sensor placement. *The Journal of the Acoustical Society of America*, 129(4):1991–2004, April 2011.
- [77] Dunant Halim and Li Cheng. Active Noise Control Experiments for an Acoustic-Structural Coupled Enclosure using Structural-Based Virtual Sensors. In *InterNoise 2014*, 2014.
- [78] Stephen J. Elliott. Distributed control of sound and vibration. *Noise Control Engineering Journal*, 53(5):165, 2005.
- [79] Oliver Nicholas Baumann and Stephen John Elliott. Global optimization of distributed output feedback controllers. *The Journal of the Acoustical Society of America*, 122(3):1587–1594, September 2007.
- [80] Wouter P. Engels, Oliver N. Baumann, Stephen J. Elliott, and R. Fraanje. Centralized and decentralized control of structural vibration and sound radiation. *The Journal of the Acoustical Society of America*, 119(3):1487–1495, March 2006.
- [81] Huiye Wang, Yi Dong, Xunjun Ma, and Minyue Lu. Distributed Diffusion FxLMS Algorithm for Multi-channel AVC System. Circuits, Systems, and Signal Processing, 43(12):8029–8045, December 2024.
- [82] Jordan Cheer and Steve Daley. Active structural acoustic control using the remote sensor method. *Journal of Physics: Conference Series*, 744:012184, September 2016.
- [83] Krzysztof Mazur and Marek Pawelczyk. Virtual Microphone Control for an Active Noise-Cancelling Casing. *Solid State Phenomena*, 248:57–66, March 2016.
- [84] Axel van de Walle, Frank Naets, and Wim Desmet. Virtual microphone sensing through vibroacoustic modelling and kalman filtering. *Mechanical Systems and Signal Processing*, 104:120–133, 2018.